AIRS

Algorithm Theoretical Basis Document

Level 1B

Part 1: Infrared Spectrometer

Version 5.0

19 October 2006

H. H. Aumann, Denis Elliot, Dave Gregorich, Steve Gaiser
Thomas Hearty and Tom Pagano

Jet Propulsion Laboratory
California Institute of Technology

Larrabee Strow
University of Maryland, Baltimore County

Table of Contents

List of Figures

List of Tables

1. Introduction

The AIRS Infrared Level 1b Algorithm Theoretical Basis Document (ATBD) describes the theoretical bases of the algorithms used to convert the output of the Atmospheric Infrared Sounder (AIRS) from engineering units to physical radiance units, to evaluate the positions of the Spectral Response Function and to provide an estimate of the noise for all 2378 spectral channels. The description of the algorithms, which convert the Level 1b measurements to geophysical units, is covered in the Level 2 ATBD.

There are many papers and reports related to the Level 1b ATBD: The most up-to-date overall description of the AIRS instrument development is given in Ref.1. The AIRS Functional Requirements Document (FRD) is in Ref. 2. The AIRS Calibration Plan (Ref.3), dated 14 November 1997, contains a description of the relevant parts of the AIRS instrument, calibration devices and calibration procedures for pre-launch characterization of parameters needed by the level 1b algorithms. The AIRS Validation Plan (Ref. 4.) describes post-launch validation of level 1b data using floating buoys, radio sondes, and satellite- and aircraft-borne instruments. The AIRS home page at JPL and the Earth Observing System (EOS) project science office at GSFC (http://airs.jpl.nasa.gov and http://eospso.gsfc.nasa.gov, respectively) post the latest versions of these plans.

The tables of coefficients required by the level 1b software which were derived from the prelaunch testing have not been changed. This insures the NIST traceability of the AIRS IR calibration, which is a fundamental requirement for a climate quality data set.

Release History:

The version number of the Level 1b ATBD are synchronized with the PGE version, which is used for routine data processing at the GSFC DAAC and at NOAA/NESDIS.

Version 1.0   November 18, 2000 prelaunch calibration

Version 2.0   Not released. No significant changes

Version 3.0   Not released. No significant changes

Version 4.0   Not released. No significant changes.

Version 5.0   is the first official postlaunch release of the level 1b ATBD

As of October 2006, the Level 1b IR data available from the GSFC DAAC from the start of data on 31 August 2002 were generated by the V5.0 PGE. The radiances from previous versions are statistically unchanged, but a number of refinements were added to cover special conditions: The changes involve:

a)   How offsets are calculated from space views;

b)   Handling of radiation-hit-induced spikes in the observed signal from the on-board calibrator;

c)   Handling and flagging detectors with significant non-Gaussian noise (cold scene noise, popping, and radiation hits); and

d)   Compiling of a set of channel properties files, each valid during a different time of the mission.

2. Instrument Overview

The Atmospheric Infrared Sounder is a high spectral resolution IR spectrometer. AIRS, together with the Advanced Microwave Sounding Unit (AMSU) and the Microwave Humidity Sounder supplied by Brazil (HSB), is designed to meet the operational weather prediction requirements of the National Oceanic and Atmospheric Administration (NOAA) and the global change research objectives of the National Aeronautics and Space Administration (NASA). The AIRS flight model calibration started in November 1998 and was completed in November 1999. Integration onto the spacecraft was completed in January 2001. Aqua, the EOS spacecraft carrying the three instruments, was launched from Vandenberg AFB on May 4, 2002. Details of the science objective are found in Ref 5.

 The AIRS instrument includes an infrared spectrometer and a visible light/near-infrared photometer. (The visible/near-IR photometer is discussed in Part 2 of the AIRS level 1b ATBD). The AIRS is a pupil-imaging infrared grating spectrometer with spectral coverage from 3.74 to 4.61 μm, from 6.20 to 8.22 μm, and from 8.8 to 15.4 μm. The nominal spectral resolution, $\lambda/\Delta\lambda\square$ is 1200, but in actuality varies as a function of frequency from 1080 to nearly 1600. The spectrum is sampled twice per spectral resolution element for a total of 2378 spectral samples. The diffraction grating disperses the radiation onto 17 linear arrays of HgCdTe detectors in grating orders 3 through 11. The position of the dispersed beam on the focal plane in the dispersed and in the cross-dispersed direction can be accurately controlled by pivoting the collimation mirror using the Actuator Mirror Assembly (AMA). The AMA proved to be critical during the pre-launch calibration, but has not been needed in orbit to date.

The scan head assembly, containing the scan mirror and calibrators. The scan mirror rotates through 360 degree every 2.667 seconds. This produces data for one scan line with 90 footprints on the ground and 6 calibration related footprints. The scan mirror motor has two speed regimes: During the first 2 seconds it rotates at 49.5 degrees/second, generating a scan line with 90 ground footprints, each with a 1.1 degree diameter FOV. During the remaining 0.667 seconds the scan mirror finishes the remaining 261 degrees of a full revolution. Routine calibration-related data are taken during this time. These consist of four independent views of Cold Space View (CSV), one view into the Onboard Blackbody Calibrator (OBC), one view into the Onboard Spectral Reference Source (OBS), and one view into a photometric calibrator for the VIS/NIR photometer.

The IR spectrometer is cooled by a two-stage radiative cooler. The temperature of the spectrometer is monitored with 6 fully redundant temperature sensors. It is fine-controlled by a temperature servo in combination with a 2.8-watt heater. This system can be set to within 0.008K. The servo heater can raise the spectrometer temperature set point by a maximum of 7 degrees above the natural orbital conditions, observed to be between 150K and 165K. The operating temperature of the spectrometer is presently controlled at 155.56K. Full radiometric and spectral calibrations were conducted prelaunch in the AIRS Test and Calibration Facility (ATCF) at 149K, 155K and 161K. These measurements show excellent radiometric and spectral calibration stability, due to the a-thermal design of the AIRS (the optical bench and grating are made from a single billet of specially annealed aluminum.). The measurements also have confirmed the 20-hour thermal time constant of the spectrometer. In-flight observations mostly support the thermal model.

The scan mirror is cooled by radiative coupling to the cold IR spectrometer, resulting in a mirror temperature approximately 50 K cooler than the spacecraft ambient, but 100K warmer than the spectrometer temperature.   The scan mirror temperature is monitored by a non-contacting sensor

located at the base of the rotating shaft, about 6" from the scan mirror surface. The temperature difference between the scan mirror surface and the temperature sensor is estimated to be less than 0.5K and temperature variations across the scan mirror surface are less than 0.05K peak-to-peak. The scan mirror is coated with silver, overcoated with a protective layer of SiO_2 by Denton using a proprietary process. The scan mirror temperature, mirror angle (relative to nadir), emissivity, emissivity non-uniformity and polarization are components of the radiometric calibration algorithm.

2.1. On-board Calibration Devices.

Routine IR radiometric calibration related data are taken while the scan mirror rotates from -49.5 degrees (relative to nadir) through 180 degrees (anti-nadir position) to +49.5 degrees. These data consist of four independent views of cold space (CSV) and one view into the Onboard Radiometric Calibrator (OBC) source. The view into the Onboard Spectral reference source (OBS) once per scan line is used as a check of the spectral stability. In-orbit the upwelling spectral radiance from the nadir footprints is used for the spectral calibration. The AIRS spectrometer is pupil imaging, i.e. detectors are located at a pupil stop of the spectrometer optics (as opposed to the detectors being at a field stop, i.e. imaging the scene on the detectors). This insures that radiometric impacts due to spatial non-uniformity in the on-board calibration targets are minimized, while impacts due to spatial non-uniformity of the scene are eliminated.

2.1.1. Onboard Radiometric Calibrator (OBC)

The OBC is a deep wedge cavity blackbody with a rectangular clear aperture 5.7 cm by 9.5 cm. The depth of the blackbody cavity is twice the diagonal of the clear aperture. The blackbody housing and cavity are made from beryllium to reduce its mass to 2 kg. The surface of the OBC wedge cavity is coated with paint with emissivity higher than 0.91. Considering multiple reflections inside the wedge, the OBC effective emissivity is estimated to be greater than 0.998.

Four semi-conductor resistance temperature sensors, T1–T4, monitor the temperature at key positions to an accuracy of 0.1 K. T1 and T2 are located on the sloping part of the wedge, T3 is located on the vertical part of the wedge, and T4 is located at the outside aperture of the OBC. The OBC is analog servo controlled at 308.0 +/- 0.01K. If a temperature sensor is found to be outside the nominal limits, a flag is raised, indicating that the calibration accuracy may be compromised. No such out-of-limits condition has been observed in orbit as of October 2006.

2.1.2. Cold Space View (CSV)

There are four consecutive views of cold space centered at 75.0, 83.0, 91.7, and 101.1 degrees from nadir-referred to as S3, S4, S1, and S2 respectively. Since the scan mirror moves continuously, the effective area used for the CSV's starts at 71.8 degrees and ends at 104.5 degrees from nadir. The use of these space views during radiometric calibration is described in Section 3.1.2 of this document.

2.1.3. Onboard Spectral reference source (OBS)

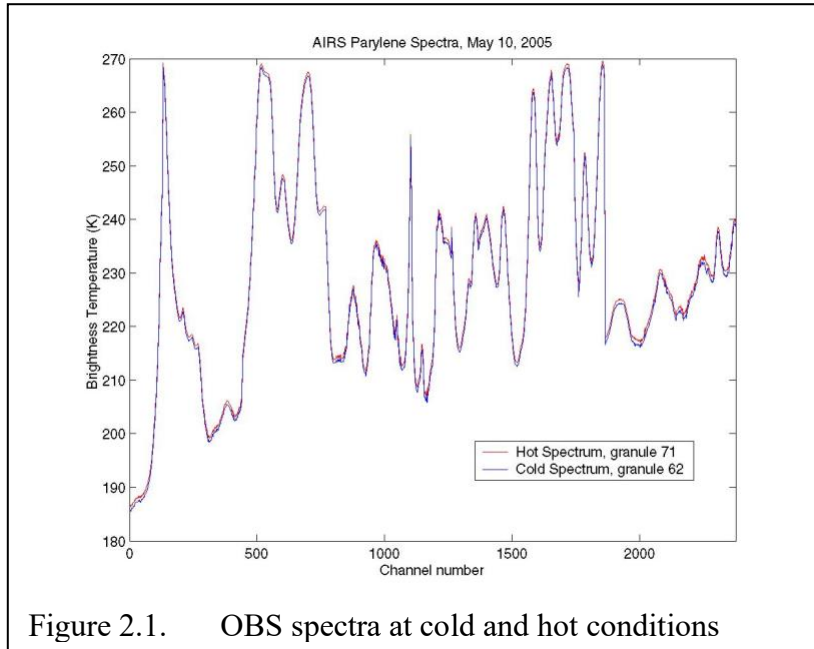A mirror coated with a thin film (about 10microns thick) of Parylene was designed as the On-Board Spectral reference source (OBS) for pre-flight testing of spectrometer functionality. Although this reference source is used occasionally for a spectral calibration check on orbit, the primary method for spectral calibration uses accurately known features in the upwelling spectral radiance as discussed section 4.3. Figure 2.1 shows the average spectra from two granules representing extremes of scan head temperature. Although the spectral features are fairly broad, they are fit to a precision better than 1% of the width (FWHM) of the spectral response function in orbit, better than the 2-3% FWHM obtained pre-launch.

Figure 2.1.   OBS spectra at cold and hot conditions

3. Radiometric Calibration

The AIRS spectrometer has 2378 spectral channels grouped in seventeen arrays. The first 15 arrays use PV detectors, the last two use PC detectors. The AIRS level 1b software reads the raw outputs of each of the 2378 channels (level 1a) for each footprint and converts them to calibrated radiances using the AIRS radiometer calibration equation. In the following section we discuss the radiometer calibration equation (algorithm) and estimate the accuracy of the calibration.

The required absolute radiometric calibration accuracy of each AIRS spectral channel, as stated in the AIRS Functional Requirements document (Ref.2.), is the larger of 3% of the radiance or 4*NEN, over the full dynamic range of AIRS from 190K to 325K, where NEN is the Noise Equivalent Radiance. Since brightness temperature uncertainties are more useful than radiance uncertainty for a temperature sounder, most of the results are expressed as temperature uncertainty.

The routine radiometric calibration of the AIRS data is performed by the Level 1b software. The output format is defined in Ref. 6. The level 1b output routinely generates quality assessment and quality flags. These indicators are used for off-line trend analysis and are also passed on to the level 2 (geophysical product generation) software.

3.1. Radiometric Calibration Equation

The accuracy of the radiometric calibration depends on accurately representing the instrument response to the scene and internal background in the calibration equations. The AIRS radiometric calibration involves scaling of the signal sensed from the scene to that of the OBC Blackbody with a correction for the nonlinear response of the detectors and a small polarization correction. The scan mirror emission plays an important role in the scan angle dependence of the infrared radiometry and have included a correction for this in the algorithm. A Mueller Matrix formalism was selected to obtain the most

accurate form of the equation. The equations reduce to a very simple analytical form with few terms, leading to minimal computational requirements for the Level 1B code and allowing for a relatively straight forward analysis of radiometric accuracy errors. Details of the prelaunch calibration are found in Ref.7. The calibration equations are found in Ref.8.

Key to the precise prelaunch radiometric calibration were the large aperture blackbody (LABB) and the cold reference, SVBB, the space view blackbody (Fig. 3-1). The LABB, and the SVBB are traceable through there design details and the thermometry to National Institute of Standards and Technology (NIST). The LABB temperature sensors were calibrated by NIST prior to installation into the LABB. The temperature precision of the LABB is approximately 0.01K with a stability of 0.01K. The uncertainty of the temperature of the first surface is less than 0.03K, with all other surfaces less than 0.1K. With more than 90% contribution from the first surface, we expect the temperature uncertainty to be better than 0.05K.

Figure 3-1   AIRS SVBB and LABB Internal Geometry
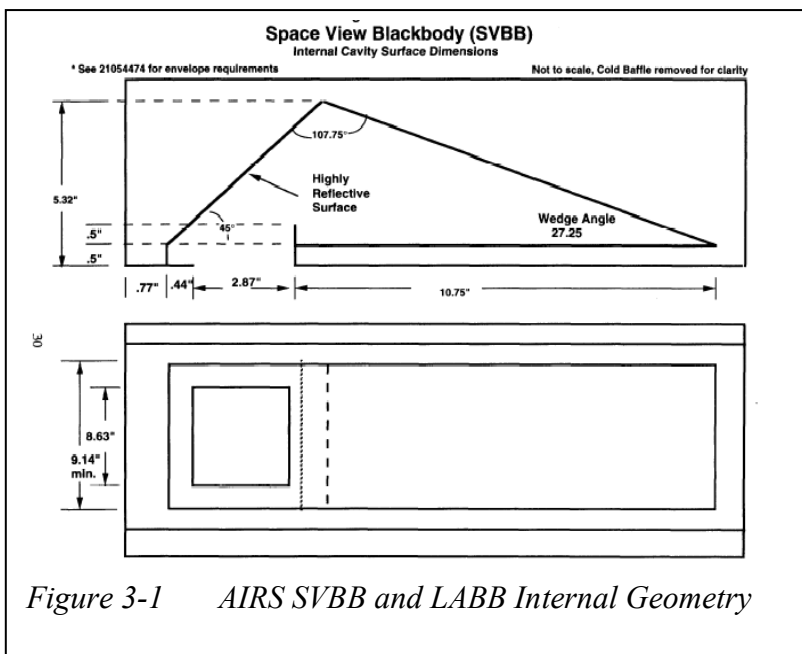
The LABB output is NIST traceable through contact thermometry of the NIST calibrated temperature sensors, but not through actual radiance measurements. We therefore rely on knowledge of the surface properties of the LABB and a model of its emissivity. The LABB is a wedge cavity design, considerably larger, but otherwise similar in its basic design to the OBC, but with selectable temperature between 190K and 360K. During TVAC testing it was located at a distance of 11.5" from the scan mirror. At this position its entrance aperture is large enough to fully contain four consecutive AIRS footprints. It is constructed of a specular black paint, Aeroglaze Z302, with specified reflectance of less than 13.5% for wavelengths below 6 um and less than 17.5% below 15.4 um. For the wedge angle of 27.25 degrees and the AIRS geometry, more than 6 specular reflections are required before the beam exits the cavity. The LABB emissivity is theoretically better than $(1-0.11^6)$, i.e. better than 0.99999. The SVBB was cooled with LN2.

The spectral calibration of AIRS is totally independent of the radiometric calibration. No correction is required to adjust the center frequencies of AIRS in the Plank Blackbody expression since the frequencies are stable to a few parts per million of the center frequency.

3.1.1. The Signal on the Detector

The total signal at the detector is the sum of the radiance of the scene passed through the optics and the emission of the scan mirror also passed through the optical system. In Mueller-matrix calculus, the signal is the first term of the Stokes vector **S** in the equation

$$\mathbf{S} = \mathbf{M_{sp}}\,\mathbf{M_{sm}}\,\mathbf{N_{sc}} + \mathbf{M_{sp}}\,\mathbf{N_{sm}} \tag{1}$$

Where:

$\mathbf{M_{sp}}$ = Mueller Matrix for the Spectrometer
$\mathbf{M_{sm}}$ = Mueller Matrix for the Scan Mirror
$\mathbf{N_{sc}}$ = Radiance of the Scene
$\mathbf{N_{sm}}$ = Emission of the Scan Mirror

The Mueller matrix for a linear diattenuator with fast axis θ (relative to the x-axis) and reflectance q and r in the s and p directions, respectively, is given by[2]:

$$\mathbf{M} = \frac{1}{2}\begin{vmatrix} q+r & (q-r)\cos2\theta & (q-r)\sin2\theta & 0 \\ (q-r)\cos2\theta & (q+r)\cos^2 2\theta + 2\sqrt{(qr)}\sin^2 2\theta & \left(q+r-2\sqrt{(qr)}\right)\sin2\theta\cos2\theta & 0 \\ (q-r)\sin2\theta & \left(q+r-2\sqrt{(qr)}\right)\sin2\theta\cos2\theta & (q+r)\sin^2 2\theta + 2\sqrt{(qr)}\cos^2 2\theta & 0 \\ 0 & 0 & 0 & 2\sqrt{(qr)} \end{vmatrix} \tag{2}$$

In what follows, we define θ to be the orientation, and q and r to be the reflectances in the perpendicular and parallel directions, respectively, of the scan mirror; t, v, and δ are the same parameters for the spectrometer.

Assuming the scene to be unpolarized, the radiances of the scene and scan mirror are given, respectively, by the vectors:

$$\mathbf{N_{sc}} = \begin{vmatrix} N_{sc} \\ 0 \\ 0 \\ 0 \end{vmatrix} \qquad\qquad \mathbf{N_{sm}} = \frac{1}{2}P_{sm}\begin{bmatrix} \varepsilon_s + \varepsilon_p \\ (\varepsilon_s - \varepsilon_p)\cos2\theta \\ (\varepsilon_s + \varepsilon_p)\sin2\theta \\ 0 \end{bmatrix} \tag{3}$$

where P_{sm} is the Plank blackbody radiation function evaluated at the temperature of the scan mirror.

Consider the first term of (1), the contribution from the scene:

$$\mathbf{M_{sp}}\,\mathbf{M_{sm}}\,\mathbf{N_{sc}} = \mathbf{M}(t,\ v,\ \delta)\ \mathbf{M}(q,\ r,\ \theta)\ [N_{sc}\ 0\ 0\ 0\ ]' \tag{4}$$

Because the scene is assumed to be unpolarized, multiplying the matrix for the scan mirror times the scene produces a vector. (Note that if the scene has polarization, we need to carry the additional elements in the vector[3]).

$$\mathbf{M_{sp}M_{sm}N_{sc}} = \frac{1}{2}N_{sc}\mathbf{M}(t,\ v,\ \delta)\begin{vmatrix} (q+r) \\ (q-r)\cos 2\theta \\ (q-r)\sin 2\theta \\ 0 \end{vmatrix}$$

$$M_{sp}M_{sm}N_{sc} = \frac{1}{2}N_{sc}[M(t,v,\delta)]\begin{bmatrix} (q+r) \\ (q-r)\cos 2\theta \\ (q-r)\sin 2\theta \\ 0 \end{bmatrix} \qquad (5)$$

Multiplying out the matrix gives Equation 6.

$$M_{sp}M_{sm}N_{sc} = \frac{1}{4}N_{sc}\begin{bmatrix} (q+r)(t+v)+(q-r)(t-v)(\cos 2\theta\cos 2\delta+\sin 2\theta\sin 2\delta) \\ (q+r)(t-v)\cos 2\delta+((t+v)\cos^2 2\delta+2\sqrt{(tv)}\sin^2 2\delta)(q-r)\cos 2\theta+((t+v-2\sqrt{(tv)})\sin 2\delta\cos 2\delta)(q-r)\sin 2\theta \\ (q+r)(t-v)\sin 2\delta+((t+v-2\sqrt{(tv)})\sin 2\delta\cos 2\delta)(q-r)\cos 2\theta+((t+v)\sin^2 2\delta+2\sqrt{(tv)}\cos^2 2\delta)(q-r)\sin 2\theta \\ 0 \end{bmatrix} \qquad (6)$$

The second term in (1), the contribution from scan mirror emission, is the same, with q, r replaced with the scan mirror emissivity in s and p polarizations, ε_s, ε_p. This gives Equation 7.

$$M_{sp}N_{sm} = \frac{1}{4}P_{sm}\begin{bmatrix} (\varepsilon_s+\varepsilon_p)(t+v)+(\varepsilon_s-\varepsilon_p)(t-v)(\cos 2\theta\cos 2\delta+\sin 2\theta\sin 2\delta) \\ (\varepsilon_s+\varepsilon_p)(t-v)\cos 2\delta+((t+v)\cos^2 2\delta+2\sqrt{(tv)}\sin^2 2\delta)(\varepsilon_s-\varepsilon_p)\cos 2\theta+((t+v-2\sqrt{(tv)})\sin 2\delta\cos 2\delta)(\varepsilon_s-\varepsilon_p)\sin 2\theta \\ (\varepsilon_s+\varepsilon_p)(t-v)\sin 2\delta+((t+v-2\sqrt{(tv)})\sin 2\delta\cos 2\delta)(\varepsilon_s-\varepsilon_p)\cos 2\theta+((t+v)\sin^2 2\delta+2\sqrt{(tv)}\cos^2 2\delta)(\varepsilon_s-\varepsilon_p)\sin 2\theta \\ 0 \end{bmatrix} \qquad (7)$$

Substituting equations (6) and (7) into (1) produces an expression for the Stokes vector **S**. Since we are not analyzing polarization we are only interesting in the intensity, the first term of **S**:

$$S_o = 1/4\ P_{sm}\ [(\varepsilon_s+\varepsilon_p)(t+v) + (\varepsilon_s-\varepsilon_p)(t-v)(\cos 2\theta\cos 2\delta + \sin 2\theta\sin 2\delta)] \quad + \qquad (8)$$
$$1/4\ N_{sc}\ [(q+r)(t+v) + (q-r)(t-v)(\cos 2\theta\cos 2\delta + \sin 2\theta\sin 2\delta)]$$

We would like to express this in terms of the mirror average reflectance and average spectrometer transmission and polarization.

First note the identity:

$$\cos\theta\cos\delta + \sin\theta\sin\delta = \cos(\theta-\delta) \qquad (9)$$

and define the terms R, T, ε, p_r, p_t, and p_ε such that:

$$q + r = 2R; \; q\text{-}r = 2Rp_r, \; \text{where } p_r = (q\text{-}r)/(q+r)$$
$$t + v = 2T; \; t\text{-}v = 2Tp_t, \; \text{where } p_t = (t\text{-}v)/(t+v)$$
$$\varepsilon_s + \varepsilon_p = 2\varepsilon; \; \varepsilon_s - \varepsilon_p = 2\varepsilon p_\varepsilon, \text{ where } p_\varepsilon = (\varepsilon_s - \varepsilon_p)/(\varepsilon_s + \varepsilon_p) \qquad (10)$$

Substitution gives:

$$S_o = N_{sc}\{RT + RTp_rp_t \, cos2(\theta\text{--}\delta)\} + P_{sm}\{\varepsilon T + \varepsilon Tp_\varepsilon p_t \, cos2(\theta\text{--}\delta)\} \qquad (11)$$

Now use:

$$\varepsilon = 1 - R$$
$$p_\varepsilon = [(1\text{-}q)\text{-}(1\text{-}r)] \,/\, [(1\text{-}q)+(1\text{-}r)] = -(q\text{-}r)\,/\,(2\text{-}(q+r)) = -2Rp_r\,/\,2(1\text{-}R)$$
$$p_\varepsilon = -Rp_r\,/\,\varepsilon \qquad (12)$$

Substituting again gives the expression for the intensity on the detector:

$$S_o = N_{sc}RT\{1 + p_rp_t \, cos2(\theta\text{--}\delta)\} + P_{sm}RT\{\varepsilon/R - p_rp_t \, cos2(\theta\text{--}\delta)\} \qquad (13)$$

S_o is the total radiance seen by the AIRS instrument at the detector from the scene and the scan mirror, as modulated by the polarization.

3.1.2. Scene Radiance

The basic approach for AIRS radiometric calibration is to perform a gain and offset (two point) correction. This first involves subtracting the space view signal from the Earth view signal every scan to correct for detector and electronic drift. For AIRS, the space views are near $\theta = 90°$, and $N_{sv} = 0$. Using this and the identity $cos2(\pi/2\text{--}\delta) = -cos2\delta$ allows us to express the net radiance measured at the detector as:

$$S_{sc} - S_{sv} = N_{sc}RT\{1 + p_rp_t \, cos2(\theta\text{--}\delta)\} - P_{sm}RT \, p_rp_t \, [cos2(\theta\text{--}\delta)+cos2\delta] \qquad (14)$$

The AIRS radiometric response is calibrated during pre-flight testing by viewing a Large Area Blackbody (LABB) at multiple temperatures simultaneously with a Space View Source (SVS). The measured response from AIRS and the radiance of the LABB were fit to a second order polynomial such that at every temperature and for every scan, i, and footprint, j, the following equation is true to within curve fit errors:

$$N_{sc,i,j}\{1 + p_rp_t \, cos2(\theta_j\text{--}\delta)\} - P_{sm} \, p_rp_t \, [cos2(\theta_j\text{--}\delta)+cos2\delta] =$$

$$a_o(\theta_j) + a_{1,i}\,(dn_{i,j} - dn_{sv,i}) + a_2\,(dn_{i,j} - dn_{sv,i})^2 \tag{15}$$

Solving for the radiance of the scene, we get the radiometric calibration equation:

$$N_{sc,i,j} = \frac{a_o(\theta_j) + a_{1,i}(dn_{i,j} - dn_{sv,i}) + a_2(dn_{i,j} - dn_{sv,i})^2}{1 + p_r\,p_t\,\cos 2(\theta_j - \delta)} \tag{16}$$

where

$N_{sc,i,j}$	=	Scene radiance of the ith scan and j^{th} footprint
i	=	Scan Index
j	=	Footprint Index (1 to 90)
θ	=	Scan Angle. $\theta = 0$ is nadir.
$dn_{i,j}$	=	Raw Data Number for the Earth View for the ith scan and j^{th} footprint
$dn_{sv,i}$	=	Space view counts offset. This is an algorithmic combination of the raw space view digital numbers.
a_o	=	Radiometric offset. This is nonzero due to polarization and is scan angle dependent.
$a_{1,i}$	=	Radiometric gain. This term converts DN to radiance based on the radiometric gain as determined using the OBC blackbody.
a_2	=	Nonlinearity Correction
$p_r p_t$	=	Polarization Product. This is the product of the polarization factors from the scan mirror and the spectrometer, respectively
δ	=	Phase of the polarization of the AIRS spectrometer

The $dn_{i,j}$ are measured directly, as are the scan angles θ. The polarization parameters $p_r p_t$ and δ were determined pre-flight, as are the nonlinearity coefficients a_2 (Ref 8.). The calculation of the offset counts $dn_{sv,i}$ is somewhat complicated and is discussed in section 3.3.

By inspection of equation (15) and we can express the radiometric offset a_o as

$$a_o(\theta_j) = P_{sm}\,p_r\,p_t[\cos 2(\theta_j - \delta) + \cos 2\delta] \tag{17}$$

where

P_{sm} = Planck function evaluated at the scan mirror temperature

And by evaluating equation (16) for the OBC view (that is, by substituting N_{OBC} for N_{SC}, and $\theta_{OBC} = 180$ degrees for θ_j), solving for $a_{1,i}$ gives

$$a_{1,i} = \frac{N_{OBC,i}(1 + p_r\,p_t\,\cos 2\delta) - a_o(\theta_{OBC}) - a_2(dn_{obc,i} - dn_{sv,i})^2}{(dn_{obc,i} - dn_{sv,i})} \tag{18}$$

14

3.2. Application of Pre-Flight Calibration Data To the Radiometric Calibration Equation

Examination of the radiometric transfer Equations 16, 17, and 18 indicates that several terms must be known to derive the radiance. Many of these terms are derived from the instrument telemetry. The scan mirror radiance, P_{sm}, is obtained by evaluating the Planck function at the scan mirror temperature which is determined using telemetry from a non-contact temperature sensor in a small on-rotation-axis cavity in the back of the mirror. Likewise, the OBC emission N_{OBC} is calculated from the Planck function and pre-flight measurements of OBC emissivity using telemetry from the four temperature sensors. The scan angle θ_j is read out directly from the encoder on the scan motor. The data number from the earth scene, $dn_{i,j}$ is obtained directly from the instrument analog-to-digital (A/D) converter for each channel when viewing the Earth scene. The space view counts offset, $dn_{sv,i}$ involves a slightly more complicated algorithm as discussed in section 3.3. The remaining terms $N_{OBC,i}$, $p_r p_t$, δ, and a_2 are obtained from pre-flight calibration and are also discussed below.

3.2.1   Polarization Terms $p_r p_t$ and δ

Equation 17 gives an expression for the offset, a_o, in terms of the product of the polarizations of the scan mirror and the spectrometer, $p_r p_t$. We have three ways of determining this product.

The first way simply uses the radiometric intercept, a_o obtained during the fit of LABB data during radiometric calibration as mentioned above. Since the calibration is performed at a known scan angle of $\theta = 0°$ and $\theta = 40°$, we can solve directly for the $p_r p_t$ term.

$$p_r p_t = \frac{a_o}{P_{sm}[\cos 2(\theta_j - \delta) + \cos 2\delta]} \tag{20}$$

The second way obtains the $p_r p_t$ term directly from measurement of the instrument and scan mirror polarization. Polarization data were obtained during system level testing in Thermal Vacuum of the AIRS instrument polarization. An off-axis section of a paraboloidal mirror is used to project the image of a target aperture onto the field stop of the AIRS instrument. The polarization of the optical beam entering the AIRS entrance pupil has four possible states, selectable by a choice of one of four positions of a filter wheel containing wire grid polarizers in three different orientations, plus one open position. The filter wheel is in close proximity to the target aperture, reducing the clear aperture requirements on the polarizers. The polarizers and the targets are actively cooled with liquid nitrogen to a temperature less than 150 K to reduce the effects of thermal background signal on the polarization measurements. Figure 3-2 shows the measured polarization obtained during T/V testing.

The third technique calculates a theoretical polarization based on component measurements of S and P transmission and reflection made on witness samples during the development phase. Grating polarization was calculated using a numerical electromagnetic model. Mirror data were obtained from measurements made by Mike McDonald at MIT Lincoln Labs (Ref. 10). The system polarization model uses these data in a Mueller matrix formalism to arrive an overall determination of the system polarization. The modeled results are shown in Figure 3-2. We do see some departure in the longer wavelengths from the measurements. This deviation is included in the uncertainty modeling.
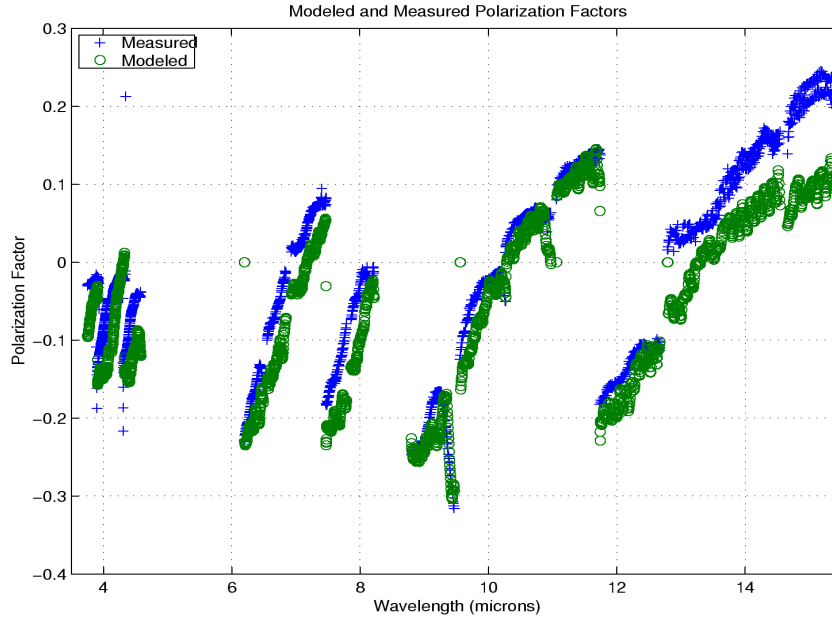
Figure 3-2   Measured and modeled polarization for the AIRS instrument

Figure 3-3 shows the results of multiplying the measured and modeled polarization by the MIT mirror data to give the prpt product. We overlay with this the prpt as calculated from the radiometric intercept at nadir and 40° scan angles as described above (equation 20). The radiometric data confirms the polarization data and model and gives us 4 data sets from which to determine the prpt term. We have chosen to use the average of the measured and modeled data sets as our at-launch prpt values. We carry the difference of these two sets as the uncertainty.

Figure 3-3   Polarization product $p_r p_t$ obtained 4 different ways

Results show that the measured phase, δ, for most channels is about 10 degrees, but varies considerably from channel to channel. The modeled phase is zero for all channels due to the al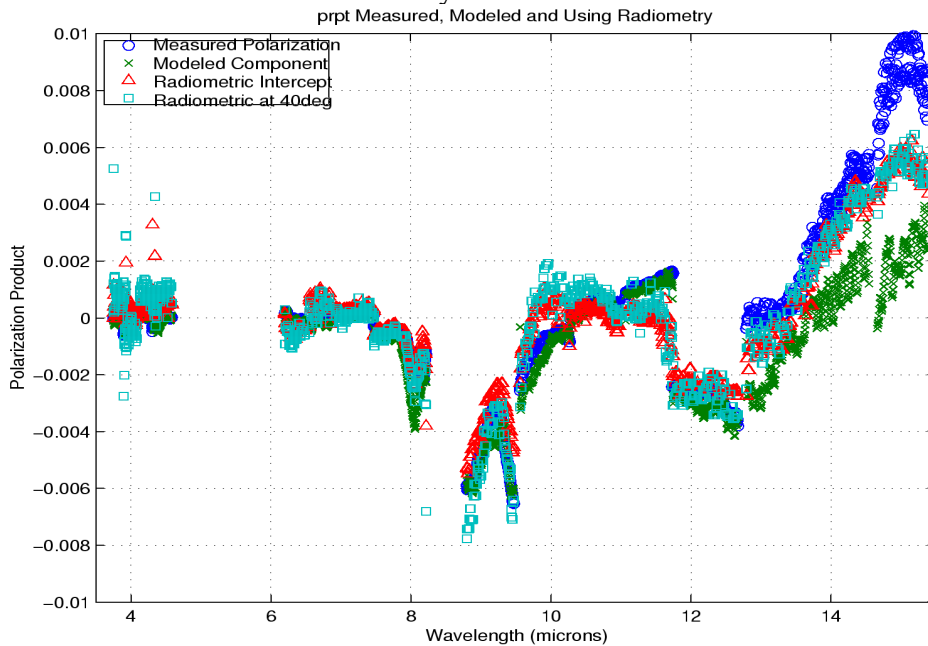ignment of all optical elements in the optical path and the absence of phase retardance in the system. We have chosen to not believe the measured phase because the phase becomes indeterminate when the polarization is small and cannot be accurately measured. Therefore, we use the modeled phase, $\delta = 0$, for all channels.

3.2.2. Nonlinearity Term, a_2

During T/V testing, the AIRS viewed the LABB and the SVS. The radiometric response was measured by stepping the LABB over multiple temperatures: 205 K, 220 K, 230 K, 240 K, 250 K, 265 K, 280 K, 295 K, and 310 K. At each level, the LABB was temperature stabilized and more than 100 scans of AIRS data acquired. The center of the LABB was carefully located and signal levels ($\Delta dn = dn_{i,j} - dn_{sv,i}$) were averaged over scans and available footprints. Values of a_2, and placeholder values of a_0 and a_1 were then calculated by performing least-squares fits to the polynomial

$$N_{LABB} = a_0 + a_1 \Delta dn + a_2 \Delta dn^2$$

where N_{LABB} is the radiance of the LABB as derived from its temperatures sensors.

We have only one OBC blackbody on the AIRS instrument; therefore, we cannot update the nonlinearity in orbit. As a result, we must use the second order term from the pre-flight calibration using the LABB. We define the nonlinearity as the fractional radiance contribution from the second order term evaluated at the scene temperature as follows

$$NL = \frac{a_2 (dn - dn_{sv})^2}{a_o + a_1 (dn - dn_{sv})} \qquad (26)$$

The resulting nonlinearity from two separate measurements is plotted in Fig. 3-4 at a scene brightness temperature of 280K. We see less than 1.5% nonlinearity with better than 0.2% repeatability of the measurement for tests taken four days apart and at different scan angles.
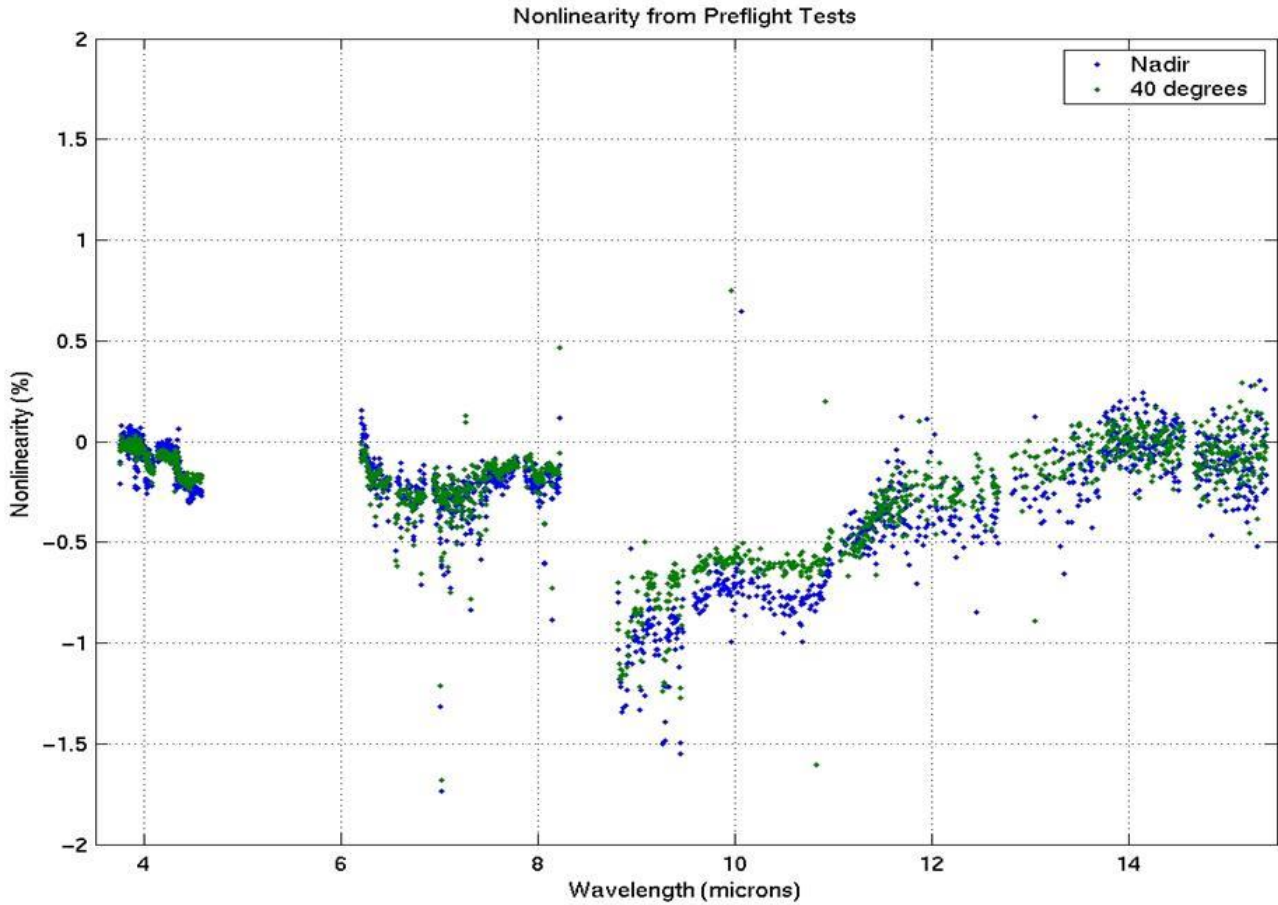
Figure 3-4   AIRS Non-Linearity

3.2. 3. OBC Temperature and Effective Emissivity

As described in section 2.2.1, the OBC has four temperature sensors. The measured OBC temperature T_{OBC} is calculated as a linear combination of these four temperatures:

$$T_{OBC} = \tau_1 T_1 + \tau_2 T_2 + \tau_3 T_3 + \tau_4 T_4 \tag{25}$$

The four weights τ_i have been given values $\tau_1=0.45$, $\tau_2=0.45$, $\tau_3=0.09$, and $\tau_4=0.01$ based on the positions of the sensors and based on the recommendations of AIRS thermal engineers. Going into the pre-flight data analysis it was expected that this temperature would be accurate, but comparison of the calculated N_{OBC} calculated from

$$N_{OBC} = a_o + a_1(dn_{OBC}-dn_{sv}) + a_2(dn_{OBC}-dn_{sv})^2 \tag{22}$$

did not agree well with the N_{LABB}, so it was decided to represent the error as an offset term. That is, it was decided to recalculate the N_{OBC} as the planck function calculated for $T_{OBC}' = T_{OBC} + \Delta T$, where ΔT

18

is some constant offset TBD. Because the OBC is operated over an extremely narrow range of temperatures (controlled to 307.92 +/- 0.05K), the constant offset model works as well as any other mathematical representation.

In a physical sense what we would like to derive is the temperature offset ΔT and emissivity of the OBC blackbody. In a practical sense we do not have enough information to solve for both independently. Therefore, we assume a temperature correction based on expectations from the OBC blackbody and consider the rest to be due to the emissivity and residual uncertainty in the temperature and other unknown terms. We call the emissivity/temperature residual term the "gain correction factor" because it is not the true emissivity of the OBC blackbody.

The gain correction factor ε_{OBC} is then defined as the ratio between the observed radiance and the planck function calculated at the effective temperature:

(23)

$$\varepsilon_{OBC} = \frac{N_{OBC}}{P_{OBC}(T_{OBC}+\Delta T)}$$

where P_{OBC} is the planck radiance of the OBC blackbody at the temperature $T_{OBC} + \Delta T$. By iterating the temperature offset ΔT until the gain correction term is near 1.0 for all channels, it was found that a value ΔT=0.3K works best, meaning that the temperature of the OBC as measured directly by its thermometers is low by 0.3 K. This 0.3 K correction term is reasonable when compared to the calibration offsets for the OBC blackbody temperature sensors during their calibration, the OBC blackbody thermal environment, and the electronic design of the temperature sensor readout. The gain correction factor is shown in Figure 3-5 and is within 0.2% of unity for almost all channels. The terms "OBC gain correction" and "OBC effective emissivity" are used interchangeably.
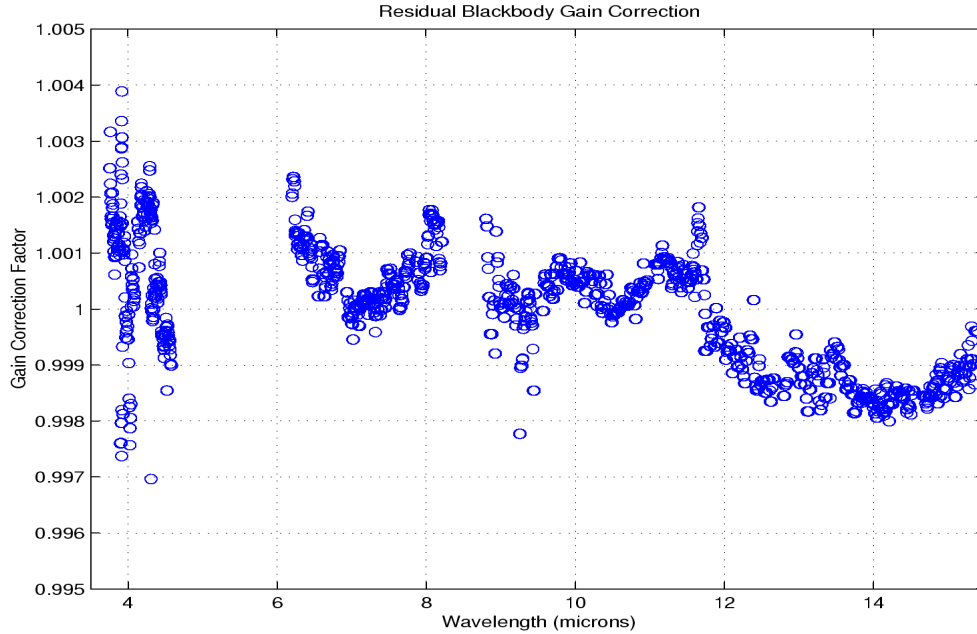
Figure 3-5   OBC Gain Correction Factor

In-flight, the radiance of the OBC blackbody ($N_{OBC,i}$ in equation 18) is obtained then from the OBC gain correction factor and the OBC blackbody temperature telemetry for every scan:

$$N_{OBC,i} = \varepsilon_{OBC}\ P(T_{OBC,i}+0.3\ K) \tag{24}$$

3.3.   Space-View-Processing

Every signal measured by AIRS viewing is the combination of the signals from the target radiance, from the thermal emission of the AIRS instrument, and from the electronics offset. The signal, in data numbers, associated with thermal emission and electronics offset $dn_{sv,I}$ varies with time and is determined from views of cold space. Associated with each cross-track scan are four space view measurements called S1, S2, S3 and S4. The space views occur while the AIRS boresight vector is at 91.7, 101.1, 75.0, and 83.0 degrees from nadir, respectively, while the Earth horizon is at 61 degrees from nadir. Space view S2 is followed by a view of the blackbody at a 180-degree scan angle. The cycle repeats every 2.67 seconds.

Figure 3.6. The difference between the four spaceviews can be measured, but they are less than 0.1K equivalent for a 250 K scene.

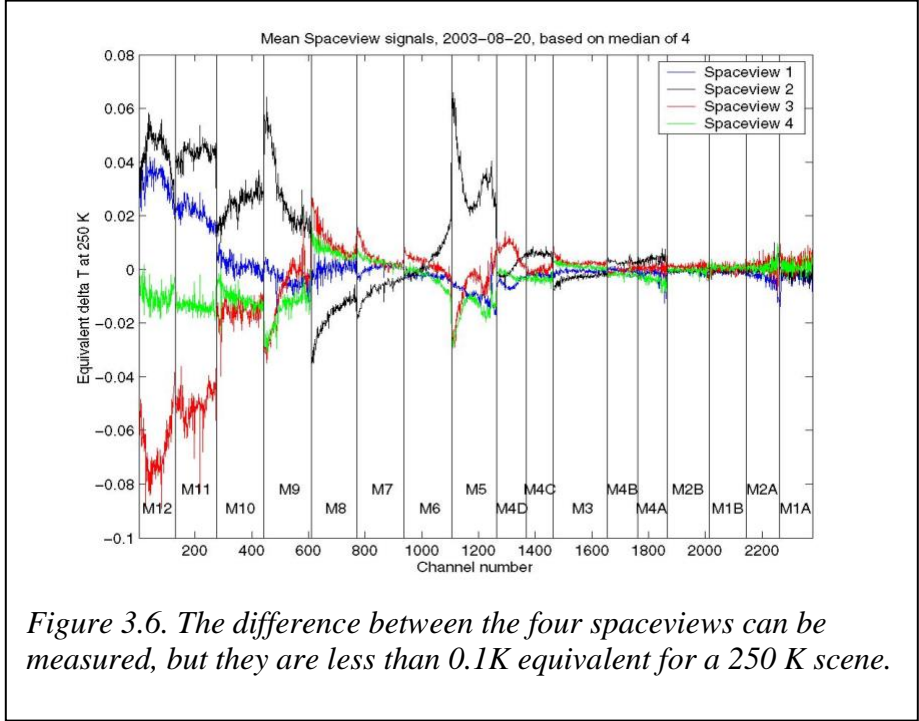Prelaunch it was concern that there might be some contamination of the space views due to contributions from the Earth's limb, possibly requiring that S3 be excluded from offset calculations. Figure 3.6 shows the actual observed biases of the four space views as a function of AIRS channel number. While real biases are observed, their magnitudes are less than 0.1K (for a 250K scene), a small effect. Furthermore, the four space views do not show a monotonic change as one moves away from the Earth's limb, contradicting the pre-flight expectation. For these two reasons, all four space views are used to calculate the offset signal.

In order to reduce or eliminate possible effects caused by outliers (especially spikes caused by radiation events), the $dn_{sv,i}$ are calculated from medians of consecutive space views. That is, for each group of adjacent space views S3, S4, S1, and S2, a median value of the signal is calculated. To further reduce the radiance error due to the uncertainty in the offset, the $dn_{sv,i}$ are calculated by performing a linear fit (in time) to the five space view medians before the scan of interest and the five space view medians after the scan of interest. This method, calculating medians of groups of four space views, and fitting linearly in time to ten such medians, forms the basis of the AIRS IR offset calculation, but several factors discussed in the following complicate the implementation.

In order to support the analysis of potential degradation of the calibration due to scan mirror contamination, the mean, max and min space view signal determined from each detector for each data granule are saved.

3.3.1. Moon-in-view

At accurately predictable times the moon is visible in AIRS space views. This occurs roughly six months in each year, for two to three days of those months, for one or two granules each orbit of those days. When this happens the moon is usually present in only one of the four space views, and the median algorithm successfully excludes it as an outlier. But it can also happen that the moon is present in two consecutive space views, which would badly skew the median. Consequently an algorithm has

been implemented to identify space views containing moonlight contamination and exclude them from the median calculations.

15 channels were selected for identification of moon contamination, one from the middle of each PV detector array. Consider the four space views that are to go into a median calculation. For each of the 15 "moon channels", the minimum signal (in counts) is found for the four space views. Each of the other three space view signals is then expressed as a difference from this floor signal level. If any of these three space view differences is greater than some multiple (currently 5) times the channel's noise, then that footprint is identified as possibly moon-contaminated, based on that moon channel. If a certain number (currently ten or more) of the moon channels identify the same footprint as possibly moon-contaminated, then that footprint is excluded from the median calculation.

3.3.2. DC Restore

The analog output (voltage) of all 2378 AIRS channels are sampled simultaneously using a sample-and-hold capacitor for each channel. The conversion for analog to digital is done sequentially. A large fraction of the signal from PV modules M3-M10 is due to the background, i.e. the infrared radiation from the spectrometer, and electrical offset due to dark currents. In order to more accurately (and faster) digitize the analog signal, the analog signal is read as the difference between the sample-and-hold capacitor and a DC restore capacitor of each channel. The DC restore capacitor discharges slowly with time following an exponential decay, with time constants varying from an estimated mean of 90 minutes in M8 to over 1000 minutes in M5. Because of the way the readout electronics are connected, this results in the digitized signal decreasing with time (for all measurements) in modules M3-M5, and results in the signal increasing with time for modules M6-M10. For this reason the DC restore capacitors are refreshed periodically, in an event referred to as the DCR ("DC Restore"). The DCR time is on-orbit commandable, but was set to 20 minutes during prelaunch testing. The DCR occurs between scans (that is, at the end of the dwell period associated with viewing S4, but before S1) and results in a discontinuity in signal level between S4 and S1. The times of these DCRs are identified in downlink telemetry. It was discovered during instrument testing that, for DC restored channels, the first space view following a DCR (S1) is always invalid. For this reason it is excluded from the median calculations.

3.3.3. Fitting Across Discontinuities

The linear fit in time to the ten space view count medians is straightforward when the data vary smoothly, but when a step occurs in the data (due to a data dropout, a DCR or pop, additional steps are required in the level 1b algorithm. When a DCR is indicated in telemetry, it is known to have occurred between scans; that is, it is known to have occurred after S4 and before the immediately following S1. All channels in modules M3-M10 experience a discontinuity in their signal levels at this time, precluding a simple fit. So for each of these channels, two one-sided fits are performed first. The median of the two space views immediately prior to the discontinuity (S3 and S4, filtered for possible moon contamination) is calculated, as are medians for the nine preceding groups of four space views. In the event that a pop is detected for this channel sometime during the nine scans before the DCR, then

only medians after the pop are used. To these median values (ten nominally, absent any pops) a straight line is fitted in time, and an offset dn_{pre} is calculated corresponding to the time of the discontinuity.

Likewise, a fit is also performed to the space views following the DCR discontinuity. The median of the two space views immediately after to the discontinuity (S1 and S2, filtered for possible moon contamination) is calculated, as are medians for the nine following groups of four space views. In this case S1, immediately following the DCR, is invalid, so the median of the two space views immediately following the DCR is simply the value of S2. In the event that a pop is detected for this channel sometime during the nine scans after the DCR, only medians before the pop are used. To these median values (ten nominally, absent any pops) a straight line is fitted in time, and an offset dn_{post} is calculated corresponding to the time of the discontinuity.

The difference dn_{pre} - dn_{post} is then added to space views following the discontinuity and a fit to ten [now smoothed] medians is calculated as described above. Finally the difference dn_{pre} - dn_{post} is subtracted back off the fit values following the discontinuity. Discontinuities introduced by pops are handled similarly (difference added in, fit to, and subtracted back off), but with two differences First, pops detected by the Quality Assurance (QA) algorithm occur during the scene portion of a scan. That is, they occur between space views S2 and S3 instead of between space views S4 and S1. Second, the magnitude of the discontinuity correction comes from the pop detection QA rather than from the two one-sided linear fits used with DCRs. The scan line during which a pop occurs is identified in the level 1b output.

3.3.4. Scan Angle Dependent Radiometric offset

The AIRS radiometer calibration equation includes a scan angle dependent radiometric offset term proportional to the amount of polarization of the scan mirror and the spectrometer

$$a_o(\theta_j) = N_m \bullet p_r p_t \bullet [\cos 2(\theta_j - \delta) + \cos 2\delta] \qquad \text{Eq 3-6}$$

where

$a_0(\theta_j)$ = Scan angle dependent offset due to polarization

θ_j = Scan mirror angle for the jth footprint, relative to nadir

N_m = Radiance of a blackbody at the scan mirror temperature, T_{sm}

$p_r p_t$ = Product of the polarization factors of the scan mirror and spectrometer respectively (dimensionless).

δ = Phase of the polarization of the AIRS spectrometer (Ref. 8)

Although the radiance from the scan mirror at 250K is small, it cannot be neglected. Eq.3-6 was validated during prelaunch calibration.

The spectrometer polarization phase (δ) was measured during prelaunch calibration at LMIRIS (now BAE Systems) as well as $p_r p_t$. But because of some confusing results, it was decided to ignore the phase term in the Level 1b software used at launch. A reanalysis of the polarization measurements was performed in early 2004. However, the effect of using the resulting phase data (as opposed to ignoring δ) was negligible in the calibrated radiances. So the phase term remains zero in the level 1b software.

3.4. Noise and Precision

Characterization of the instrument precision and noise are important to quantification of random errors. Systematic biases are the only terms considered in the absolute radiometric accuracy discussed in section 3.4. While the majority of the instrument noise is uncorrelated, we find a small but measurable amount of correlated noise that must be included in the radiometric accuracy allocations.

3.4.1. Instrumental Random Noise

The random noise was characterized pre-launch and during special on-orbit tests. The pre-launch noise characterization was performed by acquiring instrument digital output while viewing calibration targets at known temperatures. In this test, the AIRS scan mirror is locked at the calibration target for 20 minutes while data are collected. For AIRS, data were acquired while viewing the Space View Blackbody (SVBB), and the Large Area Blackbody (LABB). Radiometric sensitivity is expressed as the Noise Equivalent Temperature Difference (NEdT) for a scene temperature of 250K. On-orbit the NeDT is measured for every granule by analyzing the standard deviation of the OBC and SV measurements for each of the 135 scan line in one granule. The NEdT for AIRS is measured by interpolating the noise while viewing cold space and the OBC at 308K according to equation 27.

$$ NEdT = \frac{Gain \times \sqrt{\frac{N_{sc}}{N_{OBC}}\left(\sigma^2_{dn\_OBC} - \sigma^2_{dn\_SV}\right) + \sigma^2_{dn\_SV}}}{\partial N_{sc}/\partial T} \qquad (27) $$

where
NEdT =   Noise Equivalent Temperature Difference (K)
σ =   Standard Deviation of counts for scene (sc), OBC, and Space View (SV)
N   =   radiance of scene (sc), and OBC
Gain =   Radiometric Gain (W/m^2-sr-um / counts)
T   =   Temperature (K)

The NEdT's for AIRS are shown in Fig. 3-7 pre-flight and in-orbit. These NEdT's are on a per-pixel basis. There are fewer "outliers" in the in-orbit data set due to better optimizations in the combination of A and B detectors for a given channel.
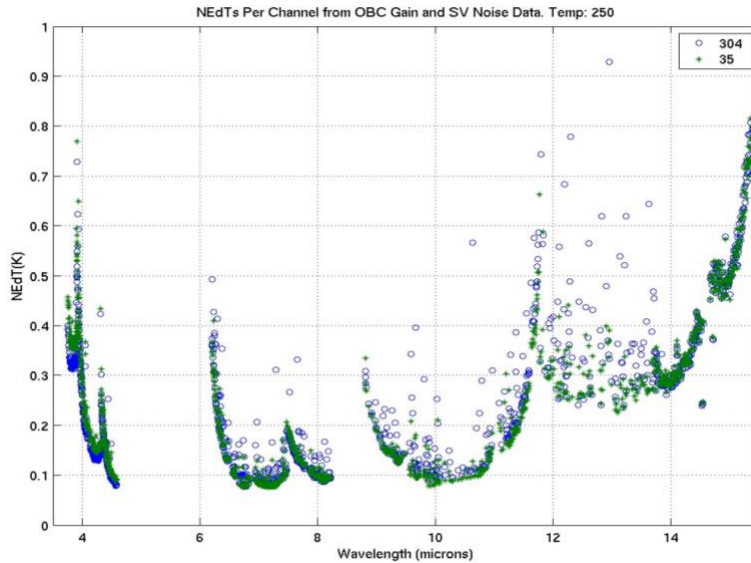
Figure 3-7   AIRS NEdT's at 250 K

3.4.2. Instrumental Correlated Noise

Figure 3-8 shows the noise amplitude (1 sigma) for the 17 AIRS detector modules obtained while viewing cold space during thermal vacuum testing. Through analysis we have determined what fraction of the noise is correlated amongst the channels; this is also shown in the figure. Correlated noise does exist in some AIRS modules, with M1, M2, M4, and M8 showing the greatest levels. Worst case, these levels are about 2x lower than the nominal noise. This is not surprising, since all detectors in a readout share common circuitry. The random noise will be higher at non-zero scene radiances and should reduce the impact of correlated noise.
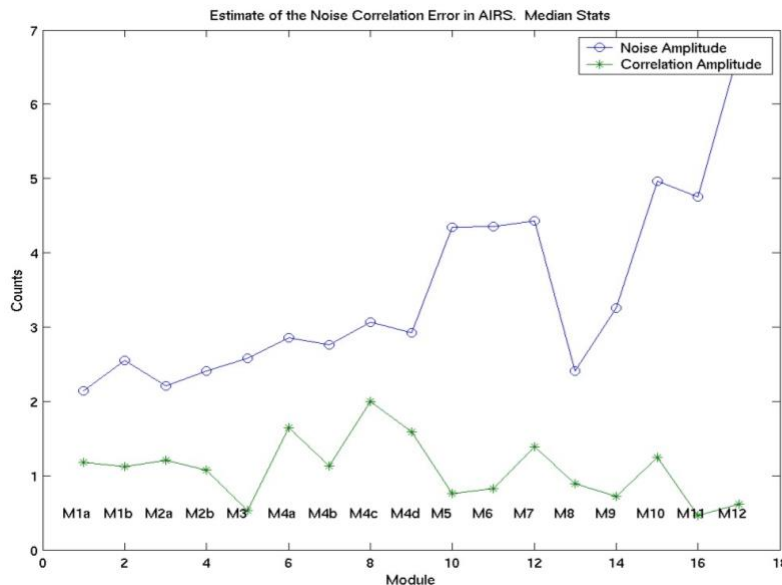
Figure 3-8   AIRS Random and Correlated Noise

3.4.3. Instrument Precision

In order to assess the precision or repeatability of the AIRS measurements, the Level 1B algorithms were exercised on an independent data set (other than the ones used to derive the calibration coefficients) to derive the observed radiance of the target. The LABB temperature varied from 205 K to 310 K; the data were obtained three days after the day the data were taken to derive the coefficients. The AIRS was placed on a rotary table in thermal vacuum and moved to view the LABB at a scan angle of 40 degrees. This angle tests the effectiveness of the scan angle corrections in the radiometric transfer equations. The temperature of the LABB was determined from the derived radiance and compared to the expected temperature. The residual systematic errors are shown in Figure 3-9 for the LABB temperature of 265 K. We see less than 0.2 K residual errors at all temperatures measured for most channels.
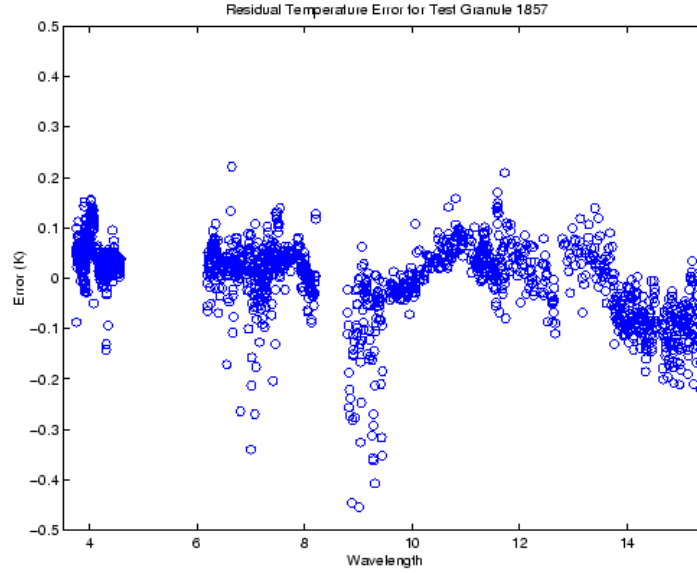
Figure 3-9   Residual Temperature Error for AIRS

3.4.4. Absolute Radiometric Uncertainty

The radiometric uncertainty is the absolute radiance error between any AIRS measurement during the course of the mission and the NIST standard temperature sensors in the ground LABB. Radiometric uncertainty only includes the bias of the instrument, and not the random noise. We can determine the uncertainty in the radiometry by applying variance analysis on the radiometric transfer equations (16, 17, and 18). This will give us only those errors that are directly attributable to the calibration equation. We can add to this the uncertainty of the AIRS transfer standard, the Large Area Blackbody (LABB), to arrive at an overall measurement uncertainty5.

$$\partial N_{SC}{}^2 = \left(\frac{\partial N_{SC}}{\partial p_r p_t}\Delta p_r p_t\right)^2 + \left(\frac{\partial N_{SC}}{\partial T_{sm}}\Delta T_{sm}\right)^2 + \left(\frac{\partial N_{SC}}{\partial \varepsilon_{sm}}\Delta \varepsilon_{sm}\right)^2 + \left(\frac{\partial N_{SC}}{\partial \varepsilon_{OBC}}\Delta \varepsilon_{OBC}\right)^2 + \left(\frac{\partial N_{SC}}{\partial T_{OBC}}\Delta T_{OBC}\right)^2 + \left(\frac{\partial N_{SC}}{\partial a_2}\Delta a_2\right)^2 + \left(\frac{\partial N_{SC}}{\partial dn}\Delta dn\right)^2 \qquad (28)$$

Rather than solve for the equation analytically, we can apply the variance directly to the radiometric equation and calculate the change in radiance. This was performed in a computer model with the following assumptions for the error terms. All terms entered are 3-sigma, resulting in a 3-sigma uncertainty.

3.3.4.1. Error Terms

Polarization: $p_r p_t$: The first primary error term is the uncertainty in the product of the polarization factors of the scan mirror and spectrometer. We cannot explain the differences in Figure 3-3 between the various approaches, and carry the difference between the radiometric offset term at nadir and the average of the modeled and component offset terms as the radiometric error.

Scan Mirror Temperature and Emissivity: $\Delta T_{sm}, \Delta \varepsilon_{sm}$: The AIRS scan mirror temperature is monitored using a non-contacting temperature sensor located at the base of the rotating shaft. The temperature sensor, though stationary, is radiatively coupled to the scan mirror and thermally decoupled from the rest of the scanner assembly. Thus the scan motor or other heat inputs don't affect the mirror temperature measurement. The uncertainty in the scan mirror temperature is estimated to be less than 0.5K by design. Models executed by the instrument contractor estimate the uncertainty to be less than 1K. The scan mirror emissivity uncertainty at launch and any scan-angle-dependent uncertainties are carried in the polarization term. The effect of emissivity non-uniformity and its potential calibration effect is discussed in Appendix 3. The degradation effects are not included in this model so the results represent at-launch expectations.

OBC Temperature Uncertainty: ΔT_{OBC}: The temperature of the OBC Blackbody is monitored by four temperature sensors located in and around the OBC. We have seen fluctuations on the order of $\pm 0.05K$ in the blackbody temperature, but we believe the uncertainty on this measurement to be on the order of $\pm 0.01K$. All other biases on this term come out of the emissivity calibration of the OBC.

OBC Gain Correction Term: $\Delta \varepsilon_{OBC}$: A 0.3K offset was applied during the calibration to match the radiances of the OBC and the external LABB. The uncertainty of this correction are contained in the gain correction term, ΔOBC. The 0.3 K offset is due to the fact that the temperature sensors on the OBC were calibrated using a different bias current from the bias used for measurements in flight. This situation is explained in detail in AIRS Design File Memo #594. We have included all of the gain correction as an error; i.e. $\Delta \varepsilon_2 = 1-\varepsilon_{OBC}$.

Nonlinearity: Δa_2: The uncertainty in the nonlinear term is taken to be the difference in the values obtained for this term for the nadir and 40 degree tests as shown in Figure 3-4.

Non-Random Instrumental Noise: Δdn: This term represents the instrumental noise while viewing the target. By convention, we do not include the random noise terms in the absolute radiometric uncertainty estimate, since they cancel in the analysis of large numbers of observations. 6. We include here the non-random, correlated instrumental noise component as a full radiometric error. It is not known what effect correlated noise has in the Level 2 retrieval processing; further simulation is planned.

3.4.4.2. Error Results

Figure 3-10 shows the results of predicting the radiometric errors based on the assumptions in the previous section. The major contributors are the correlated noise, the polarization term, and the gain. The correlated noise is the highest of these, yet is the most uncertain in its contribution on the radiometry. For all channels, we see the 3-sigma radiometric error to be less than 0.18K. These errors will later be combined with the predicted LABB radiometric accuracy to arrive at an estimate of the AIRS radiometric accuracy.

Overlaid on the prediction are module averages of the observed repeatability error measured pre-flight with a 265 K blackbody and shown in Figure 3-10. The error is the difference between the derived temperature of the LABB using the calibration coefficients and the true temperature obtained from the LABB temperature sensors.
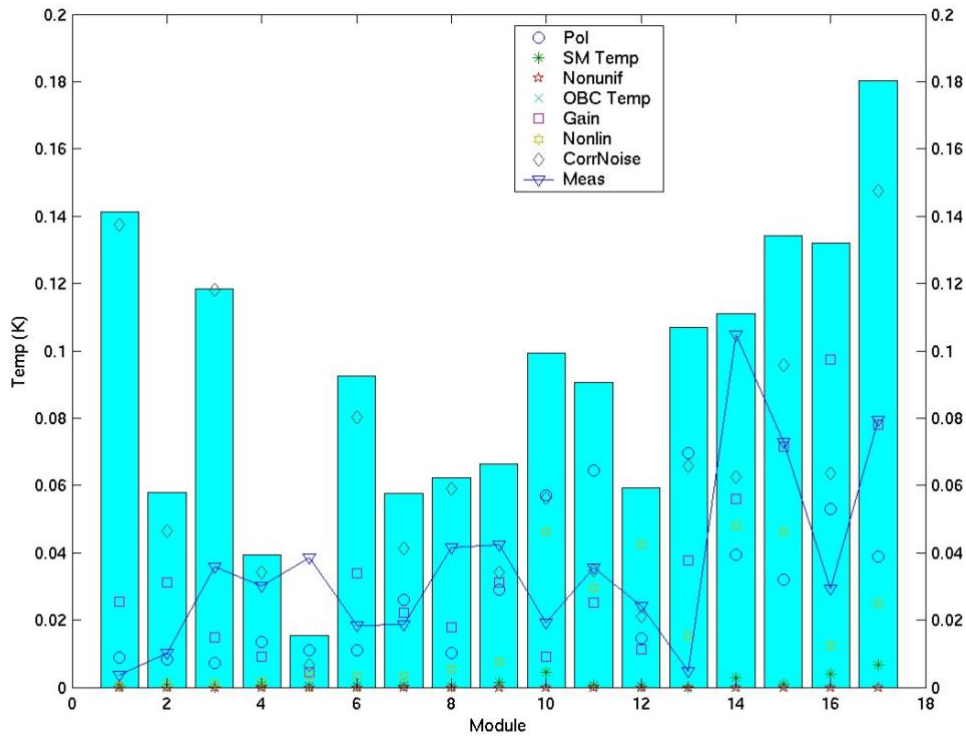
Figure 3-10   Modeled Radiometric Error (3σ) And Pre-Launch Repeatability

Our estimate of the absolute uncertainty of the LABB and SVBB of better than 0.05 K combined with the better than 0.18 K radiometric errors gives us a 3-sigma total radiometric uncertainty of better than 0.2K for AIRS. The uncertainty of any single measurement of the analysis of a small number if measurements needs to include the random noise at the scene temperature.

The AIRS instrument was designed to produce absolute accuracy radiances of "climate quality". The essential accuracy of the first principles based estimate of the absolute has by now been confirmed, The 0.2 K (3-sigma) absolute accuracy has been validated using comparisons with the RTGSST for scene temperatures between 285 K and 305 K (Ref. 11) . Absolute accuracy at the 100 mK level has been verified using five underflights with the SHIS (Ref.12.) and observation from Concordia Station at Dome C (Ref. 13). Analysis using the first three years of AIRS RTGSST observations indicate that any trend in the absolute calibration is less than 16 mK/year (Ref. 11).

4. Spectral Calibration

The AIRS spectrometer has a spectral resolution R= $\nu/\Delta\nu$ nominally equal to 1200, where ν is the Spectral Response Function (SRF) centroid frequency in wavenumber units, and $\Delta\nu$ is the SRF full width at half its maximum response (FWHM). The AIRS Radiative Transfer Algorithm (AIRS-RTA[1]) needs extremely accurate SRFs for each AIRS channel to ensure that uncertainty in the calculated radiances due to SRF uncertainties are much less than the AIRS random noise. The SRF of each channel is characterized by the absolute position of the spectral response centroid and the shape of the spectral response (normalized to unity) relative the centroid. Base on the effect of SRF shape and position uncertainty on the accuracy of the upwelling spectrum calculated by the forward algorithm, the AIRS Functional Requirements Document (FRD) (Ref 2,) called for a knowledge of channel centroid frequencies, ν, to within 1% of $\Delta\nu$ at all times. The FRD also stipulates that the are not to vary by more than 5% of $\Delta\nu$ over any 24-hour period.

The routine determination of the centroids of the SRF of all channels is the Level-1B spectral calibration task. This done once per data granule (6 minutes of data) and the result is saved in the level 1B record. Determining the shape of these SRF's using a Bruker Instruments Model IFS-66V laboratory grade FTS interferometer was a pre-launch calibration task and therefore is not part of the Level 1B algorithms. Details of the pre-launch calibration are given in Ref 14. The SRF's used for the AIRS-RTA are available as 2378 x 256 arrays at http://asl.umbc.edu/pub/airs/srf/srfhdf.html.

Pre-launch it was anticipated that the AIRS-RTA would use the SRF centroids generated by the level 1b spectral calibration, i.e. the AIRS-RTA would track any daily variability or long-term trend in the centroids. By September 2002, five months after the launch of EOS Aqua and at the start of the AIRS routine data gathering phase it became obvious that the stability of the AIRS spectral centroids far exceeded the ability of the spectral calibration to determine the centroids using data from one granule. It was therefore decided to define a "standard set" of frequencies, freq_std, which are used by the RTA, independent of the frequency calibration provided by the level 1b software. The centroids deduced from each granule and the uncertainties are saved as the "measured frequencies" and the frequency measurement uncertainties are included in the level 1b output.

4.1. Conceptual Approach

The AIRS in-orbit infrared spectral calibration is absolute, using identified features at known spectral locations in observed upwelling radiance spectra. It is based primarily on three components:

1) Focal plane detector assembly models;
2) A spectrometer grating model; and
3) Upwelling radiance spectra [both measured and modeled].

---

[1] The AIRS-RTA is a subroutine in the Level 2 software, which takes the state of the atmosphere (temperature and moisture profile, surface temperature and emissivity, and the vertical profile of Ozone and CO2) and the SRF centroids and returns the corresponding brightness temperatures for the 2378 AIRS channels.

The focal plane detector assembly models specify the position of each AIRS infrared detector on the focal plane assembly, relative to the other detectors. A different focal plane detector assembly model is used for each of the three spectrometer thermostat set-points (149K, 155K, and 161K).

Three precision screws in the Actuated Mirror Assembly (AMA) can be turned in flight, finely repositioning the focusing mirror. The AMA was critical pre-launch for the optimization of alignment of the exit slit on the detector array. The AMA has not been used on-orbit.

The spectrometer grating model specifies the relation between detector SRF centroids and detector physical positions (relative to the grating and the imaging optics). This is discussed at greater length in section 4.2. The observed spectrally resolved features in the upwelling radiances provide "tie-points," allowing determination of the absolute position of the focal plane detector assembly. This is discussed at greater length in section 4.3.

The underlying assumption allowing this approach is that, for a given instrument condition (spectrometer temperature and optics alignment), the focal plane detector assembly, the relative positions of the entrance slits and relative positions of the dispersed images of the entrance slits on the focal plane remain invariant with temperature. This assumption has been born out by three types of test performed pre-launch:

A) Detector response centroids were measured before and after acoustic and vibration testing. Differences observed in detector SRF centroid (corresponding to 13% of Δv) were consistent with a shift of the focal plane assembly relative to the spectrometer optics.

B) Detector response centroids were measured in both +1g and –1g environments (to estimate the magnitude of zero-g release effects). Differences observed in detector SRF centroids (corresponding to 3% of Δv) were consistent with a shift of the focal plane assembly relative to the spectrometer optics.

C) Detector response centroids were measured repeatedly during an extended (24-hour) test simulating 14 day-night heating cycles. Again, differences observed in detector SRF centroids (this time corresponding to just 0.25% of Δv) were consistent with a shift of the focal plane assembly relative to the spectrometer optics.

4.2. Spectrometer Model

Although the AIRS spectral calibration ultimately reports the spectral calibration of all channels in wavenumber units, the calibration equations are in wavelength units, which are the natural for a grating spectrometer. In principle, the positions of the SRF centroids are given by the standard grating equation,

$$m * \lambda_i = d * (\sin(\alpha_i) + \sin(\beta_i)),\qquad\text{Eq. 4.1}$$

where m is the grating order, λ_i the wavelength of the i-th channel, $d = 77.560$ mm is the groove spacing of the grating, α_i is the angle of incidence and β_i is the angle of diffraction. Because of the layout of the AIRS entrance slits, the incidence angles a takes on one of two values, 0.55278 or 0.56423 radians, depending on which detector array is being considered.
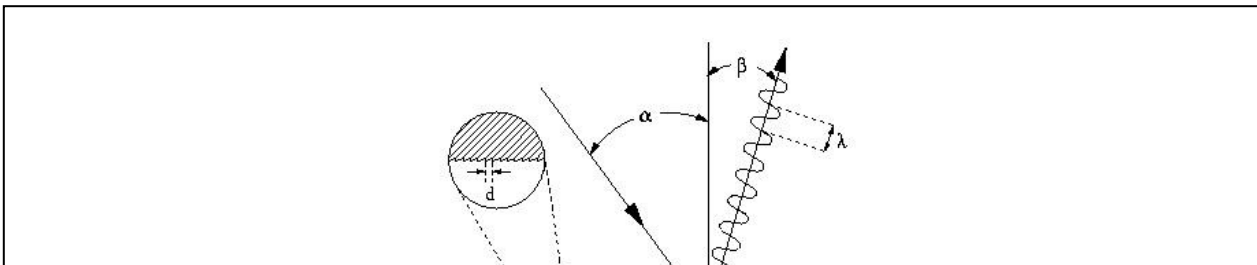
Figure 4-1   Sketch of a simple grating spectrometer

The actual AIRS spectrometer is folded with a considerably more complicated layout, but the basic equation 4-1 applies. AIRS works in grating orders 3 (at the longest wavelengths) to 11 (at the shortest wavelengths). Through the use of two spectral bandpass filters for each detector array, one covering the spectrometer entrance slit, the other directly over each detector array, and geometric optics, each detector array is guaranteed to see radiation from only one grating order.

From the geometry of the AIRS optics, the diffraction angle β^k_i corresponding to the center of the i'th detector in the k'th array is given by

$$\beta^k_i = atan(y^k_i /(F_k+ DF) \qquad\qquad (Eq.\ 4.2)$$

where F_k is the effective distance from the focusing mirror to the k'th detector array (very nearly equal to the focal length of the focusing mirror), and y^k_i is the distance (in the dispersed direction) from the optical axis to the center of the i'th detector in the k'th array. DF=0 for the pre-launch calibration. The very precise 50 µm spacing of AIRS detectors within an array then allows us to write

$$y^k_i = y^k_o + i*50\mu m + Dy_o \qquad\qquad (Eq\ 4.3)$$

Equation 4.3 is the focal plane model. This leaves us (for each "instrument temperature condition") just two parameters (per detector array), y^k_o and F_k , to determine the wavelength λi of each channel using Eq. 4.1. Dy_o =0 for the pre-launch calibration. In order two allow a more accurate fit we introduced two additional parameter for each array, a_k and ν^κ , by defining the SRF centroid frequencies as

$$\nu_i = 1/ \lambda i + a_k * (1/\lambda i - \nu^\kappa)^2 \qquad\qquad (Eq.\ 4.4)$$

The quantity ν^κ is the mean frequency of the k-th array. Equations 4.1 through 4.4 define the AIRS spectrometer calibration model. The model parameters a_k, y^k_o , Dy_o , λ^κ , DF and F_k are tabular entries in the Level 1B algorithm coefficient table. DF and Dy_o are zero initially, but are used in-orbit to fit the spectrometer model to the upwelling spectral radiance. The model accuracy meets the required $0.01*\Delta\nu$ SRF centroid position knowledge requirement

4.4. SRF Centroid Determination in Orbit

AIRS Level-1B software calculates and reports channel centroids once each data granule . This is accomplished by comparing the positions of spectral features in the upwelling radiance against pre-calculated upwelling radiance features at known frequencies.

While the AIRS spectral calibration is extremely stable as a function of temperature, the focal plane detector assembly is likely to move (relative to the rest of the optics) due to launch vibrations. It will also move due to changes in the instrument's thermal environment. To allow for this motion, two small changes must be made to the components of the spectrometer model.
The parameters DF and Dy_o allow for a focal length change and an optical axis shift common to all detectors. It is the determination of a change in focal length DF and the shift of the optical axis relative to the center of the focal plane Dy_o that makes up the in-orbit spectral calibration task.

The in-orbit SRF centroid determination method can be summarized as: Determine the positions (on the detector array assembly) at which pronounced spectral features are located and
Use this information to estimate Dy_o and DF in a least-squares sense.

The criteria for upwelling radiance feature selection, are described below.

4.4.1. Spectral Feature Fitting

The spectral features which have been selected are based on radiative transfer calculations with climatologically representative atmospheric conditions. Because radiative transfer in thermodynamically stable atmospheres is readily computable (good physics), and because absorption/emission line positions and strengths are well measured (good spectroscopy), the frequencies of the selected spectral features are also extremely well known.

The method used to determine the position of each spectral feature is as follow:

a) First, obtain an observed upwelling radiance spectrum. In principle, every AIRS spectrum could be used for wavelength calibration. In practice, only those four observations nearest nadir will be used which are reasonably cloud-free (as determined by a spectral contrast criterion, on a feature-by-feature basis). Such near-nadir, cloud free radiance spectra will be accumulated for six minutes (one granule of data) and averaged. The tremendous thermal stability of the AIRS instrument, as measured pre-launch, allows us to do this, even as the instrument crosses the terminator.
b) Then, using nominal values DF in the spectrometer model generate 11 trial frequencies sets using Dy_o = [-25, -20,… 0, 5, 10,..,25] μm.
c) Sample the pre-calculated radiance spectrum at these 11 frequency sets.
d) Calculate the correlation coefficient between each of the eleven sampled radiance spectra and the observed radiance spectrum, using the Pearson algorithm (Ref. 7).

e) Fit a parabola through the observed correlation coefficients, and determine value of Dy_o where the parabola peaks. (Note: Once the instrument has stabilized in orbit, 3 trial frequencies should be enough to determine the peak location.)

Pre-launch, the band center of each upwelling spectral feature (referred to as the "true" frequency of the feature) is converted to a position on the focal plane, using the nominal pre-launch spectrometer model. The 27 (TBD) feature shifts calculated above are added point-by-point to their pre-launch positions, producing 27 (TBD) observed feature positions.

These 27 (TBD) observed feature positions are then put through spectrometer model equations yielding 27 calculated frequencies. This process is repeated, optimizing the two parameters Dy_o and DF to minimize (in a least-squares sense) the difference between the calculated frequencies and the true feature frequencies. The downhill adaptive simplex algorithm "Amoeba" (Ref. 16) is used to find this minimum. With a global Dy_o and DF determined by the fit, a new frequency set is calculated using the spectrometer calibration equations. These frequencies are the "measured frequencies" reported by the level 1B software and archived with the data.

4.4.2. Spectral Feature Selection

Spectral features to which to fit observed radiance must satisfy a number of criteria:
1) Because these "tie-points" anchor the fit to the spectrometer grating model used for all detectors, the more features that are available to fit to, the better.
2) In order for the spectral calibration to apply equally well to all detector arrays, it is highly desirable for the spectral features to be distributed across the focal plane (evenly distributed, ideally).

1) For numerical fitting purposes, it is highly desirable to have the features be sharp (because translational fits are best done at places where radiance varies rapidly with frequency).
2) Most importantly, the calculated positions of the lines must not significantly change spectrally, under any anticipated climatological circumstances.

Table 4.1 lists the 34 spectral regions that have been identified as potential candidates for use as upwelling radiance features. A typical spectral region has 14 channels, but the number varies from eight to 26 channels.

The spectrally resolved CO_2 spectral features in the 712 to 736 cm^{-1} region of the spectrum present illustrated in Figure 4.2. is an excellent region for spectral calibration. Regions 30, 31, and 32 are included in this region. Since the lines in this region are formed high in the atmosphere, this region is much less sensitive to accidental cloud contamination.

The method used to determine suitability followed the on-orbit spectral calibration concept outlined in section 4.3.1:

a) The upwelling radiance for a US Standard temperature and moisture profile was calculated using the AIRS SRFs on a frequency grid corresponding to a nominal frequency model, and again for frequency grids corresponding to shifts in y_o by +/- 5, 10, 15, 20, and 25 microns.
b) Simulated "observed" AIRS spectra were then calculated (for each potential spectral feature) on these 11 frequency grids, for each of eight different extreme climatological conditions. The eight different climatologies were chosen to simulate anticipated variations in the upwelling radiance spectra.
c) The locations at which the correlation between the "observed" and the pre-calculated spectrum peaked (and the resulting correlation coefficients) were determined, for each spectral feature, for each climatology.
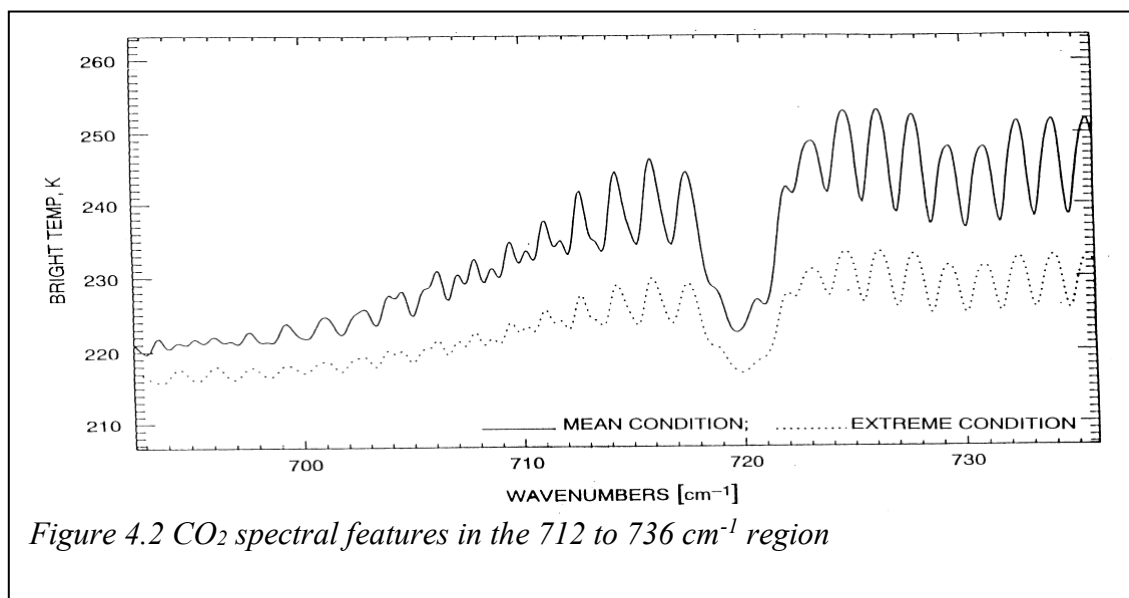

Figure 4.2 CO$_2$ spectral features in the 712 to 736 cm^{-1} region

region #	mod	LM# start	LM# end		array element start	array element end			frequency [1/cm] start	frequency [1/cm] end
					Table 4.1. Candidate region evaluation for upwelling flux spectral calibration					
1	M1a	20	27		21	28		8	2642.94	2635.35
2		34	46		35	47		13	2627.81	2614.97
3		48	56		49	57		9	2612.89	2604.37
4		95	108		96	109		14	2563.85	2550.63
5	M1b	187	200		70	83		14	2355.09	2342.81
6	M2a	256	264		9	17		9	2560.46	2551.53
7		340	356		93	109		17	2469.66	2453.08
8	M2b	461	473		98	110		13	2229.3	2218.02
9	M3	593	617		80	104		25	1397.51	1384.3
10	M4a	709	721		4	16		13	1611.43	1602.64
11		765	781		60	76		17	1571.19	1560.73
12	M4b	820	833		11	24		14	1520.19	1511.67
13		868	893		59	84		26	1489.22	1473.58
14	M4c	944	956		29	41		13	1321.81	1314.7
15		976	984		61	69		9	1303.02	1298.41
16	M4d	1035	1044		26	35		10	1258.74	1253.88
17	M5	1142	1150		27	35		9	1122.45	1118.19
18		1159	1174		44	59		16	1113.44	1105.61
19		1178	1189		63	74		12	1103.53	1097.88
20	M6	1277	1290		3	16		14	1045.11	1039.07
21		1299	1311		25	37		13	1034.94	1029.47
22	M7	1497	1524		56	83		28	952.3	941.94
23		1566	1580		125	139		15	926.26	921.15
24	M8	1648	1661		40	53		14	890.29	885.92
25		1701	1710		93	102		10	872.77	869.87
26	M9	1797	1805		28	36		9	841.4	838.21
27		1828	1840		59	71		13	829.18	824.16
28		1914	1932		145	163		19	797.01	790.58
29	M10	2029	2047		93	111		19	751.02	745.88
30		2066	2090		130	154		25	739.32	731.91
31	M11	2108	2125		5	22		18	727.13	722.04
32		2141	2159		38	56		19	717.31	712.06
33	M12	2258	2278		11	31		21	679.27	674.07
34		2346	2366		99	119		21	657.01	652.16
typical number of detectors per region =								14		
					minimum=			8		

Table 4.1   Candidate regions for spectral calibration

Statistics were calculated over the eight climatologies, providing the mean and standard deviation for the observed shifts and correlation coefficients, on a feature-by-feature basis.

Table 4-2 shows the results. The suitability flag was determined by requiring the following:

1) A mean shift of less than 1.3 microns (this is equivalent to 1.3% of the SRF FWHM)
2) A standard deviation of the shift of less than 2.6 microns, and
3) A peak correlation coefficient larger than 0.98.

Based on these criteria, 27 of the 35 candidate regions are acceptable. The spectral features were located with a mean error of 0.05 microns. This corresponds to only 0.05% of $\Delta \nu$, the SRF FWHM. All arrays except M1b and M4d contain at least one acceptable spectral feature. This test is actually a worst case test, since extreme spectra were compared to the US standard profile spectra.

4.4. Spectral Calibration Error Estimation

The uncertainty in the SRF centroid position determined by the spectral calibration algorithm has four main components:
1. The uncertainty in the spectrometer calibration model (based on pre-launch calibration), $\delta \nu_1$.
2. The uncertainty in the determination of y_o and F_o in orbit based on the finite number of spectral tie-points obtained from the upwelling spectra, $\delta \nu_2$.
3. The mismatch between the pre-calculated climatology spectra and the actual upwelling radiance, $\delta \nu_3$.

In principle, the mismatch between the calculated climatology spectrum and the observed spectrum can be made arbitrarily small by choosing enough climatology cases. The magnitudes of the rss uncertainties differ from array to array, but they are dominated by the uncertainty of the spectrometer calibration plane model, $\delta \nu_1$ (Ref. 15), which is less than 1% of $\delta \nu$.

Numerical experimentation indicated that
a) the large number of usable (minimally cloud contaminated) spectra available in one granule of data would allow the 1% of $\delta \nu$ requirement from the FRD to be met using the US Standard atmosphere spectrum globally as reference spectrum.
b) the gain of using the spectra from reference climatologies, selected by the software based the granule latitude and longitude position, was small compared to the increase in complexity in selecting the proper one.

For this reason the V4.0 Level 1b spectral calibration software uses only one reference climatology spectrum, based on the US Standard Atmosphere.

region #	mod	shift(um) mean	sigma	1.3	2nd deriv(x1000) mean	sigma	corr.coeff mean	sigma	0.98	2.6	summary good=0
1	M1a	-0.60	1.08	0	0.69	0.01	0.996	0.003	0	0	0
2		1.19	1.04	0	0.18	0.02	0.997	0.003	0	0	0
3		-0.57	0.37	0	0.30	0.01	0.995	0.005	0	0	0
4		-9.41	10.96	1	0.05	0.01	0.993	0.009	0	1	1
5	M1b	-0.73	1.14	0	0.17	0.00	1.000	0.000	0	0	0
6	M2a	-1.30	1.43	0	0.12	0.01	0.999	0.001	0	0	0
7		0.08	2.48	0	0.02	0.00	1.000	0.001	0	0	0
8	M2b	-1.86	2.63	1	0.10	0.00	1.000	0.000	0	1	1
9	M3	-0.02	0.05	0	0.12	0.00	1.000	0.000	0	0	0
10	M4a	-0.21	0.12	0	0.58	0.00	1.000	0.000	0	0	0
11		-0.05	0.26	0	0.25	0.00	0.999	0.001	0	0	0
12	M4b	0.08	0.37	0	0.32	0.00	0.999	0.001	0	0	0
13		0.17	0.17	0	0.15	0.00	1.000	0.000	0	0	0
14	M4c	-0.30	0.99	0	0.26	0.02	0.998	0.004	0	0	0
15		-0.45	0.06	0	0.32	0.00	1.000	0.000	0	0	0
16	M4d	-0.44	6.55	0	0.46	0.08	0.986	0.009	0	1	1
17	M5	-0.90	1.31	0	0.54	0.05	0.988	0.019	0	0	0
18		0.05	1.33	0	0.51	0.02	0.995	0.006	0	0	0
19		-0.07	4.51	0	0.52	0.04	0.993	0.010	0	1	1
20	M6	0.23	0.39	0	0.06	0.00	1.000	0.000	0	0	0
21		1.60	1.84	1	0.52	0.04	0.988	0.019	0	0	1
22	M7	0.91	4.00	0	0.32	0.05	0.980	0.028	0	1	1
23		-1.03	1.28	0	0.35	0.02	0.987	0.013	0	0	0
24	M8	0.13	0.15	0	0.34	0.00	0.995	0.005	0	0	0
25		-0.04	0.13	0	0.31	0.01	0.999	0.001	0	0	0
26	M9	1.17	1.55	0	0.48	0.03	0.997	0.002	0	0	0
27		-0.89	1.56	0	0.52	0.02	0.993	0.008	0	0	0
28		0.60	0.86	0	0.58	0.01	0.976	0.021	1	0	1
29	M10	-0.09	0.31	0	0.55	0.00	1.000	0.000	0	0	0
30		0.04	0.20	0	0.65	0.00	1.000	0.000	0	0	0
31	M11	-0.04	0.34	0	0.55	0.01	0.999	0.001	0	0	0
32		-0.02	1.02	0	0.51	0.00	0.999	0.001	0	0	0
33	M12	0.02	0.25	0	0.42	0.01	0.998	0.001	0	0	0
34		-0.14	1.07	0	0.48	0.01	0.997	0.003	0	0	0
		-0.05 microns									27
all array median position error							total number of good regions				

Table 4.2   US Standard and eight climatologies

The results of the pre-launch analysis have by now been confirmed with four years of on-orbit data.

Figure 4.3 The SRF centroid frequencies determined for each granule relative to a reference set in units of the width of the SRF. The requirement is 0.01.
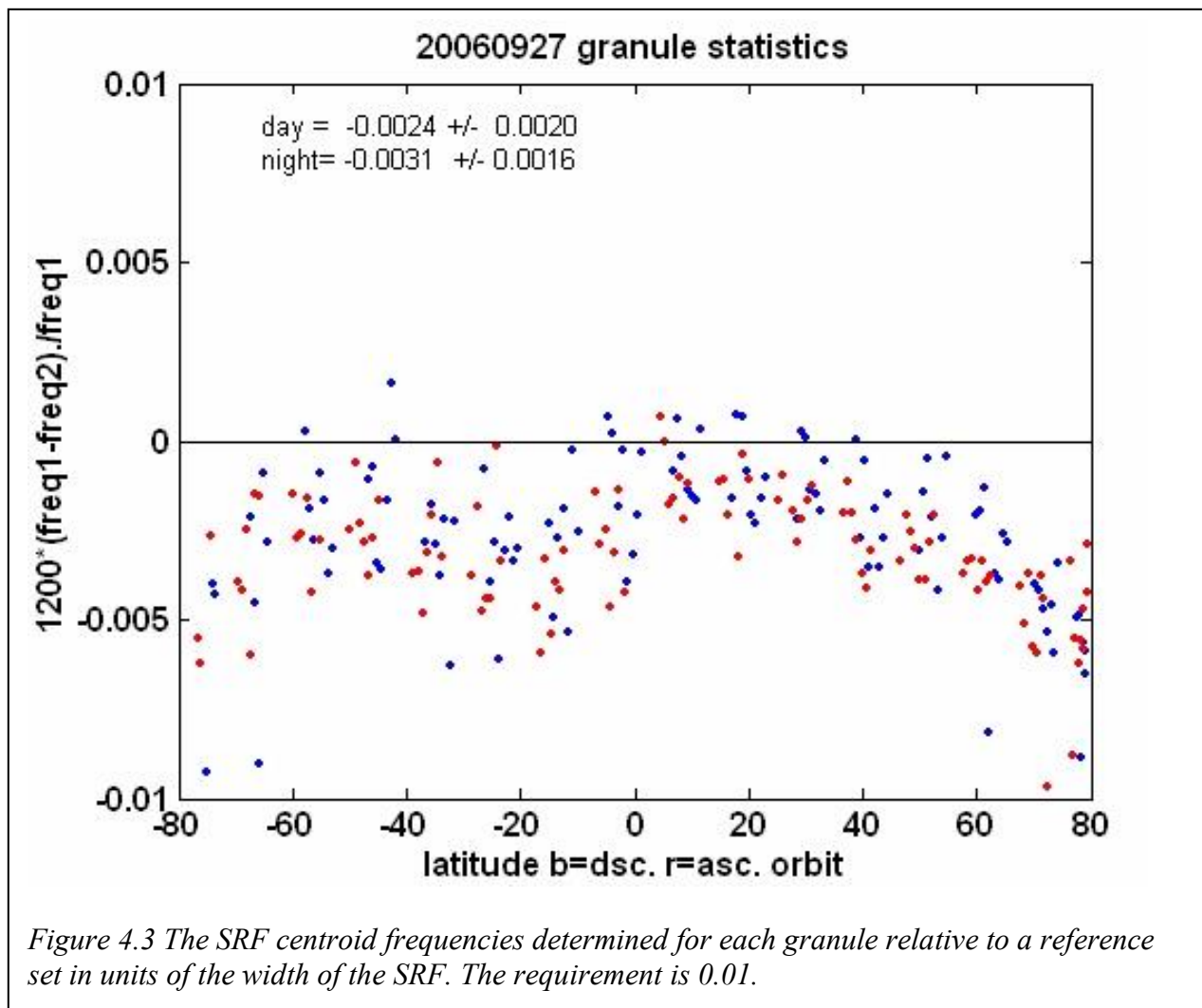
Figure 4.3 shows the difference between the SRF centroids calculated for each granule by the level 1b software, freq1, and the nominal SRF frequency, freq2, in units of δν for the 240 granules from 27 September 2006 as function of latitude. During the ascending orbits (day) the difference was -0.0031 +/- 0.0016, for the descending orbits (night) the difference was -0.0024 +/- 0.0020 for the 219 of the 240 granules where the mean surface temperature (determined under IR cloudfree conditions from AIRS) was warmer than 260 K. The frequencies are within the required +/- 1% of δν. Expressed as fraction of the frequency, the FRD requirement is +/-8 part per million per year (8 ppm).

The empirical measurement uncertainty of the individual granule measurements of 0.002*δν exceeds the 0.01*δν FRD by a factor of five. This confirms the results of the pre-launch analysis. The empirical uncertainty of the calculated frequencies for each granule approaches the difference between the calculated frequencies and the nominal frequencies.

For climate applications, where changes of 1 ppm of the frequency need to be taken into account, there are several issues with the V4.0 Level 1B spectral calibration, which need to be followed up, possibly in a future release of the software:

1) There appears to be a small (0.1% of δv) difference between ascending and descending orbits. This difference is a factor of ten below the FRD specification.
2) There is a latitude correlation in the largest deviations from zero (the nominal frequency set). The largest deviations are at the highest and lowest latitudes, where the US Standard Atmosphere spectrum is the least appropriate. The observed deviation may therefore be a calibration artifact.
3) The bump at -20 degree latitude suggests that high clouds are not properly eliminated from the spectra used for the calibration.
4) The actual SRF frequencies have shifted relative to the standard set from $+0.003*\delta v$ in September 2002 to $-0.003*\delta v$ in September 2006 (the case shown in Figure 4.3). Although the average shift was 0.15% of δv /year, additional analysis shows that the rate has slowed to about 0.1% of δv/year. The shift toward higher frequencies, expressed as fraction of the frequency is +1 part per million per year (1 ppm). The reason for this shift is at present not known.

Accurate knowledge of the SRF FWHM and the SRF wing response is important for the accurate calculation of the transmittance function in the Radiative Transfer Algorithm (RTA). Direct determination of the shape of the SRF in orbit is not possible and is not part of the Level-1B calibration algorithm. Errors in the knowledge of the SRF width and/or wing response will mimic radiometric errors, which under some conditions of high spectral contrast may become the dominant radiometric error. The routine validation program monitors radiometric biases in all channels. Biases at the 0.1K level and trends as little as 10 mK/year are detectable (Ref.11). Changes in the SRF shape would show up as radiometric errors with a pronounced spectral dependence, which mimics the spectral contrast of the upwelling radiance.

The knowledge requirement of $0.01*\delta v$ stated in the AIRS FRD was based on the requirements for weather forecasting. The AIRS level 1b software meets this requirement. For the climate applications of the AIRS radiances these requirements are about one order of magnitude to lenient. The accuracy of the spectral calibration software could be improved in a future version of level 1b software or it could be augmented by an offline spectral calibration.

5. Spatial Calibration

Each AIRS spectrum (footprints) is assigned a latitude and longitude. The static calibration of the AIRS spatial response functions were determined pre-launch. The static spatial response functions look like cylindrical like top-hats, with 1.1 degree diameter at ½ peak, 1.2 degree diameter at 1/10 peak. The mean of the centroids of the top-hats is within 80 arcsec (2% of the diameter of the beam) of the geometrical boresight of the spectrometer. Knowledge of the boresight location on the ground has to be within a 255 arc second half cone angle. The requirement is easily met by the spacecraft knowledge of the pointing vector within 12.2 arcsec (1 sigma). The spatial calibration of AIRS thus reduces to the to the determination of the common boresight.

For more critical applications, e.g. the comparison of data from different instruments, it should be kept in mind that AIRS is a cross-track scanning imager, which acquires the data while scanning cross-track. The actual spatial response function is due to the convolution of the static spatial response function with the scanning motion. This is not a level 1b calibration issue. Details regarding the validation of the dynamic spatial response function are given in Ref. 17.

5.1. Infrared Boresight Validation

The AIRS infrared boresight relative to the scan mirror axis was determined during TVAC. The level 1a software combines the scan mirror shaft encoder data and spacecraft telemetry to determine the infrared boresight. Validation that the geolocations assigned to each AIRS infrared footprint was part of the in-orbit validation software (Ref. 18), and as such not part of the level 1b software. A description of the concept is included in the following because of general interest.

The algorithm makes use of the statistics of crossings of high contrast scenes (e.g. transitions from land to ocean) to determine a longitude and latitude offset angle between the apparent boundary location and the true boundary location. If the temperature contrast between ocean and land is ΔT_{ol}, the spectrometer noise equivalent temperature per footprint is $NE\Delta T$, the angular footprint diameter is Φ, and the average angle between the cross-track scan and the coastline intersection is α, then the statistical accuracy of the cross-track position accuracy determination from n crossings is

$$\frac{\Delta\Phi(n)}{\Phi} = \frac{NE\Delta T \cos(\alpha)}{\Delta T_{ol} \sqrt{n}}$$

Eq. 5-1

For typical values of α=45 degree, NEΔT=0.2 K and ΔT_{ol}=10 K, we obtain

$$\frac{\Delta\Phi(n)}{\Phi} = \frac{0.03}{\sqrt{n}} .$$

Cross-track boresight determination (as the difference between the infrared boresight observed and the geometric boresight calculated) to within 1% of the AIRS field-of-view is achievable with 10 coastline crossings. In practice, a single orbital pass along Baja California produces about 200 coastal crossings suitable for verification of the infrared boresight. This scheme has been used successfully for ERBE and for CERES on the TRMM and EOS Terra.

6. References

1. Development and Test of the Atmospheric Infrared Sounder (AIRS) for the NASA Earth   Observing System (EOS), Paul Morse, Jerry Bates, Christopher Miller, Moustafa Chahine, Fred O'Callaghan, H. H. Aumann and Avi Karnik SPIE 3870-53, 1999.

2. AIRS Functional Requirements Document, JPL Internal Document D- 8236, Rev. 1., Oct. 1992.

3. AIRS Calibration Plan, JPL D-16821, 14 November 1997. http://eospso.gsfc.nasa.gov/calibration/plans.

4. AIRS Team Science Validation Plan, Core Products, JPL D-16822, Version 2.1 15 December 1999 ftp://eospso.gsfc.nasa.gov/sterling/Validation/AIRSplan.pdf

5. Aumann, H.H. , M.T. Chahine, C. Gautier, M. Goldberg, E. Kalnay, L. McMillin, H. Revercomb, P.W. Rosenkranz , W. L. Smith , D. H. Staelin, L. Strow and J. Susskind, "AIRS/AMSU/HSB on the Aqua Mission: Design, Science Objectives, Data Products and Processing Systems", IEEE Transactions on Geoscience and Remote Sensing, Feb 2003, Vol.41.2. pp.253-264.

6. "AIRS Version 4.0 Processing Files Description" JPL D-31231 August 2005.

7. Pagano, T.S, H. H. Aumann, D. Hagan and Ken Overoye, "Prelaunch and In-Flight Radiometric Calibration of the Atmospheric Infrared Sounder (AIRS)", (2003) IEEE Trans. Geosci. Remote Sens., Vol.41.2, pp.265-273.

8. Pagano T.S. et al., "Pre-Launch Performance Characteristics of the Atmospheric Infrared Sounder", SPIE 4169-41, September 2000.

9. "AIRS instrument polarization response: measurement methodology", G. Gigioli and T. Pagano, SPIE 3759-30, July 1999

10. AIRS Scan-mirror polarization measurements (1998) Dr. Mike McDonald, MIT Lincoln Lab, personal communication.

11. H. H. Aumann, Steve Broberg, Denis Elliott, Steve Gaiser, and Dave Gregorich ," Three years of AIRS radiometric calibration validation using sea surface temperatures", J. Geophys. Res., 111, doi:10.1029/2005JD006822

12. Tobin, David, Henry E. Revercomb, Chris Moller, Robert O. Knuteson, Fred. A. Best, William. L. Smith,Paul Van Delst, Daniel D. LaPorte, Scott D. Ellington, Mark W. Werner, Ralph G. Dedecker, Ray K. Garcia, Nick N. Cigonovich, H. Benjamin Howell, Steven Dutcher and Joe K. Taylor (2004), "Validation of Atmospheric Infrared Sounder (AIRS) Spectral Radiances with the Scanning High-resolution Interferometer Sounder (S-HIS) Aircraft Instrument", SPIE, 5571, doi:10.1117/12.566060, 383-392.

13. Walden, V.P., W.L. Roth, R.S. Stone and B Halter (2006), "Radiometric validation of the Atmospheric Infrared Sounder (AIRS) over the Antarctic Plateau", *J. Geophys. Res*. (accepted)

14. Strow, L. L., Scott E. Hannon, Margeret Weiler, Kenneth Overoye, Steven L. Gaiser and Hartmut H. Aumann, "Prelaunch Spectral Calibration of the Atmospheric Infrared Sounder (AIRS)", IEEE Transactions on Geoscience and Remote Sensing, Feb 2003, V.41,#2, 274-286

15. Gaiser, Steve L., Hartmut H. Aumann, L. Larrabee Strow, Scott Hannon and Margaret Weiler, "In-Flight Spectral Calibration of the Atmospheric Infrared Sounder" , IEEE Transactions on Geoscience and Remote Sensing, Feb 2003, V.41,#2, 287-297

16. Press, W. et al., 1992, Numerical Recipes in Fortran 77: The Art of Scientific Computing, (New York: Cambridge).

17. Elliott, D. A., Pagano, T. S., and Aumann, H. H. (2006), "The Impact Of the AIRS Spatial Response On Channel-To-Channel and Multi-Instrument Data Analyses", Proceedings of the SPIE Optics and Photonics Conference, Earth Observing Systems XI, San Diego, CA. Butler, J. J. (editor), 6296-21.

18. Dave Gregorich and Hartmut H. Aumann, "Verification of the AIRS Boresight Accuracy Using Coastline Detection", IEEE Trans, Geoscience and Remote Sensing, 4, 2, Feb 2003, pp.298-302.

19. L. Strow, S. Hannon, S. De-Souza Machado, H. Motteler, and D. Tobin, J. Geoph. Res. (2006) "Validation of the AIRS Radiative Transfer Algorithm", doi 2005JD006146RR.

Appendix 1.   Dictionary of Abbreviations

ADC   Analog to Digital converter

AIRS   Atmospheric Infrared Sounder

AMSU   Advanced Microwave Sounding Unit

ATBD   Algorithm Theoretical Basis Document

ATCF   AIRS Test and Calibration Facility (TVAC)

CSV   Cold Space View

DCR   DC Restore (of the electronics)

DN   Data Number

DOD   Department of Defense (US)

ECMWF   European Center for Medium range Forecasting

EM   Engineering Model

EOS   Earth Observing System

FOV   Field of View (projected on the ground pertaining to one dwell time)

FM   Flight Model

FRD   Functional Requirements Document

GSFC   Goddard Space Flight Center

HgCdTe   Mercury-Cadmium Telluride

HIRS   High Resolution Infrared Sounder

HSB   Humidity Sounder Brazil

IFOV   Instantaneous Field of View. Smaller or equal to the FOV.

IR   Infrared

JPL   Jet Propulsion Laboratory

MODIS   Moderate Resolution Imaging System (on EOS-Am and PM)

MSU	Microwave Sounding Unit
NASA	National Aeronautics and Space Administration
NEDT	Noise Equivalent Delta Temperature
NEN	Noise Equivalent Radiance
NIR	Near Infrared (between 1 and 3 microns)
NIST	National Institute of Standards
NOAA	National Oceanic and Atmospheric Administration
NWS	National Weather Service
OBC	On-Board Blackbody Calibrator
OBS	On-Board Spectral reference source
PC	Photoconductive Detector
PFM	Proto Flight Model
PRT	Platinum Resistance Thermometer
PV	Photo Voltaic Detector
QA	Data Quality Assessment
SRF	Spectral Response Function
TBD	To Be Determined
TVAC	Thermal Vacuum Chamber
VIS	Visible wavelength

A.2. Scan Mirror Non-uniformity Effect of the Radiometric Uncertainty

The AIRS scan mirror emissivity (averaged over the AIRS spectral coverage) is 0.015, with an estimated rms variation of less than 0.0005. The AIRS radiometric calibration uses different parts of the scan mirror for the scene, the space view and the OBC view.

Figure A.1   AIRS scan mirror profile
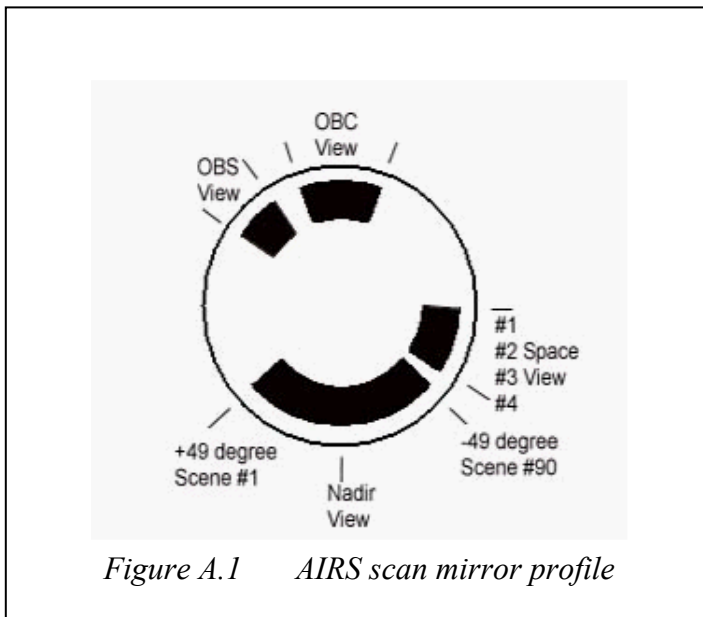
The AIRS scan mirror rotates through 360 degree every 2.667 seconds, producing one scan line with 90 footprints on the ground and 6 calibration related footprints. The entrance apertures are projected on the scan mirror, such that different parts of the scan mirror are used for calibration views and scene views. Arrays M5 through M12 use the outer most part of the scan mirror, while arrays M1 through M4 use the center part. This is illustrated in the face-on view of the scan mirror in Figure A-1, with the "track" of arrays M11 and M12 shown in black.

The AIRS level 1b calibration assumes that the scan mirror emissivity is uniform, i.e. that there is no angle dependence of the emissivity. During the pre-launch calibration a scan angle dependent correction term was measured which included polarization and any scan angle dependent emissivity effects. No emissivity non-uniformity effects were detectable, since the observed scan angle dependence agreed typically to within 0.1K with the prediction based on polarization alone.

After some time in orbit the emissivity of the scan mirror may differ from the pre-launch calibration values. Water ice deposits are not an issue, since they do not stick in the vacuum at 250K scan mirror temperature. Molecular contaminants are the most likely cause of emissivity degradation. It is very difficult to estimate the thickness of the molecular contamination due to prolonged exposure of surfaces in space. The prediction becomes even more uncertain if the surface is partially shielded, as is the case for the AIRS scan mirror. The pre-launch five years on orbit (nominally the End of Life, EOL) worst case estimate was that a layer as thick as 200A thick layer of molecular contaminants may build up on the scan mirror. This would increase the scan mirror temperature from 249 K to 261 K and increases the emissivity from 0.015 to 0.025. Since the mirror is protected inside the rotating barrel baffle, there is no preferred area of exposure to deposits. The scan mirror emissivity cancels in the calibration equation, if the emissivity was totally uniform. If the emissivity is not uniform in angle, then a time dependent trend appears in the radiometric calibration bias. The following section gives the derivation of this bias assuming a 200A thick layer of contaminants.

A1.1.1. Derivation of the radiometric effect.

We express true radiance from the scene, $N(\delta)$, as the sum of the scan angle emissivity independent term, No, a correction term, $\Delta N(\delta)$,

$$N(\delta) = No + \Delta N(\delta)$$

Assume that the scan mirror emissivity seen by a detector at scan angle δ relative to nadir is $e(\delta)$. There are 90 scene views at scan angles $-49 < \delta < +49$ degrees, space view occurs at scan angle $\delta=s$, and the OBC is viewed at scan angle $\delta=b$. The reflectivity of the scan mirror is $r(\delta)=1-e(\delta)$.

The signal $N(\delta)$ from the scene then gives the output:

$$V(\delta) * a_1 = N(\delta)*r(\delta) + e(\delta)*N(s) + Xo$$

where a_1 is the gain and we neglecting the small polarization offset and non-linearity terms. The space view signal due to the scan mirror emissivity and other background or electronic offset signals, Xo, is

$$V(s) * a_1 = N(s)*e(s) + Xo,$$

The view at the calibration blackbody produces the signal:

$$V(b) * a_1 = N(b)*(1-e(b)) + e(b)*Ns + Xo.$$

Combining the equation

$$(V(\delta)-Vs)/ (Vb-Vs) = (N(\delta)*(1-e(\delta)) + Ns(e(\delta)-e(s)))/(Nb*(1-e(b)) + Ns(e(b)-e(s)))$$

and noting that $e(\delta)<<1$ and $Ns * (e(b)-e(s)) / Nb <<1$ with the cold scan mirror we find

$$\Delta N(\delta) = Ns * (e(s)-e(\delta)) - No * (e(b)-e(\delta)).$$

As a check of the equations, note that if the scan mirror emissivity is uniform, i.e. $e(\delta)=e(s)=e(b)$, then $\Delta N(\delta)=0$, i.e. the correction term vanishes for all δ.

Expressed as rms error we may write

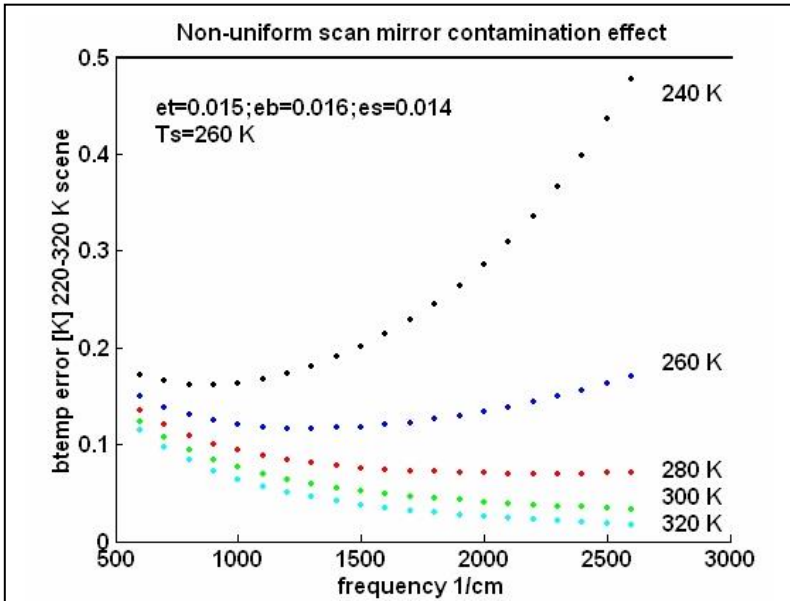$$\Delta Nrms(\delta) =((Ns * (e(s)-e(\delta)))**2 + (No * (e(b)-e(\delta)))**2)**0.5.$$

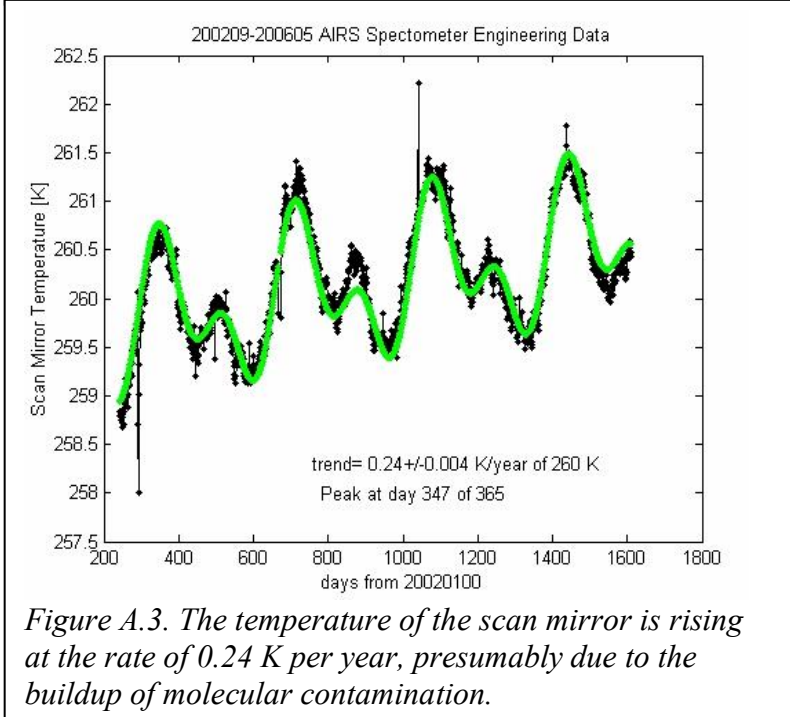Figure A.2. The effect of 200A of contamination induced scan mirror emissivitvafter five year on-orbit.

Figure A.3. The temperature of the scan mirror is rising at the rate of 0.24 K per year, presumably due to the buildup of molecular contamination.

Figure A.2. shows the magnitude of the effect predicted for 200A of contaminant and 10% non-uniformity. At brightness temperatures of 260 K and warmer the magnitude of the correction term is less than 0.2K. At lower temperatures the correction is considerably larger and strongly frequency dependent.

The temperature of the scan mirror is determined by the balance between the radiative input from the scene and the conduction to the space craft. If a 200A thick layer of molecular contaminants is deposited on the scan mirror, the temperature of the scan mirror would rise by about 12 K, i.e. 2.4 K/year. The scan mirror temperature for the past 4 years is shown in Figure A.3. It started in September 2002 at 259 K. Ignoring the seasonal 1.8 K p-p cycle due to orbital effects, the temperature is rising at the rate at the rate of 0.24 K/year. This corresponds to a 1.2 K rise in five years, a factor of 10 less than the rate deduced for a 200A thick later. The five year contamination corresponding to a 20A layer, i.e. a factor of ten less than anticipated. The error shown in Figure A.3.8 due to scan mirror contamination with the assumed 200A of molecular contamination are therefore by a factor of ten larger than the likely actual errors.

Based on the derived 20A thick layer of contamination in five years, we derive an 8, 6 and 3 mK potential shift in the calibration at 900, 1200 and 2600 cm-1 for 300 K scene, 18, 18, and 48 mK potential shift for a 240 K scene. These changes well below the random noise and would be very difficult to measure. The AIRS level 1b processing assumes that the scan mirror emissivity is uniform. The scan mirror emissivity non-uniformity term is therefore not included it in the overall radiometric uncertainty estimate developed in Section 3.3.4.1.

For climate quality data the potential effects of contamination of the scan mirror need to carefully watched.

Appendix 3. Level 1b Routine Radiometric Bias Monitoring.

Two properties which promote a set of radiances to climate quality are documented accuracy and stability. This accuracy and stability is evaluated for AIRS Level 1B calibrated radiances routinely using (obs-calc), where the calculation is based on a reliable truth. The observations are limited to locations were the AIRS spectra are identified as "cloud-free" and where the truth is reliably known from external sources. Nominally cloud-free spectra are collected routinely in the AIRS Calibration Data Subset (ACDS). This subset contains typically 70,000 nominally clear spectra per day for land and ocean. For the (obs-calc) analysis only night time clear tropical ocean spectra are used, because it was found empirically to be the region with the most reliable, stable and readily available truth data. For surface channels this truth is the Sea Surface Temperature (SST) for tropical oceans, deduced from the drifting buoys and distributed by NCEP as the Real Time Global SST (RTGSST) on a 0.5 degree grid. For atmospheric channels we use the state of the atmosphere given by ECMWF on a one degree grid.
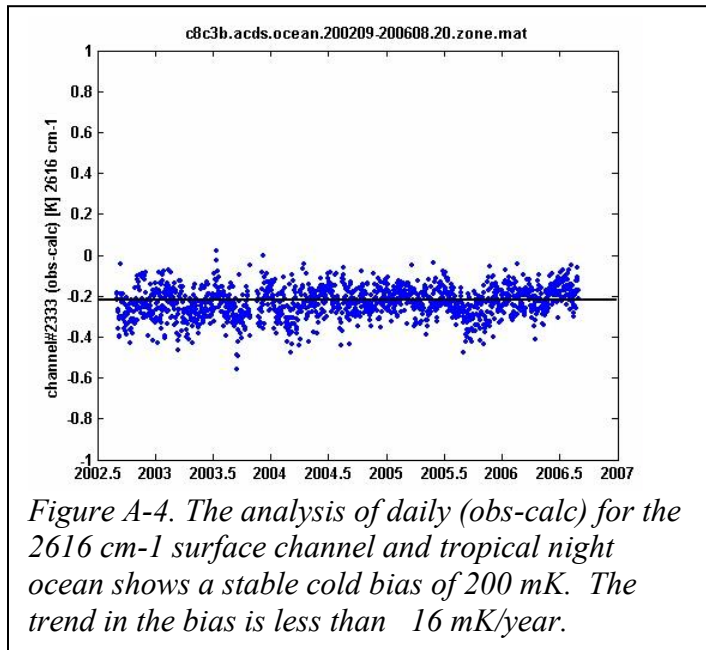

Figure A-4. The analysis of daily (obs-calc) for the 2616 cm-1 surface channel and tropical night ocean shows a stable cold bias of 200 mK. The trend in the bias is less than 16 mK/year.

Figure A.4. shows the results of the daily (obs-calc) for the 2616 cm-1 window channel under IR clear night tropical ocean conditions. There is a cold bias of about 0.2 K which is attributed to residual cloud contamination. Analysis of the first three years of AIRS data this bias has been extremely stable, with a trend of less than 16 mK/year in 300 K (Ref. 11).

The calculation of the expected brightness temperature, calc, is relatively straight forward for surface channels, since the necessary water correction is small and can be inferred from water vapor continuum sensitive AIRS channels. The routine monitoring of AIRS bias is done for surface channels in eight of the seventeen AIRS detector arrays. This more than suffices for the monitoring of the instrument performance related to the stability and accuracy of the calibration. For non-surface channels the calc procedure is much more complex and relies on the availability of an accurate Radiative Transfer Algorithm (RTA) algorithm and the accurate knowledge of the entire state of the atmosphere. The principle use of this information until 2004 was ECMWF. Details of the validation of the AIRS-RTG using (obs-calc) for all channel with ECMWF as the truth are given in Ref. 19.

Appendix 4. Frequently Asked Questions (FAQ)

In the following we answer "Frequently Asked Questions" regarding the AIRS Infrared Spectrometer: Radiometric Calibration, Spectral Calibration and in-orbit Calibration Validation. This includes all questions raised by reviewers of the level 1b IR ATBD in February 1997 and March 2000 and additional ones posed by members of the user community.

1. Questions about the radiometric calibration

How will the degradation of the OBC emissivity be monitored?

The OBC is a full aperture wedge cavity. The angles of the sides of the wedge cavity design are designed to utilizes multiple reflection from inside surfaces. For the AIRS design there are six "reflections" from surfaces with diffuse reflectivity of about 11%. This results in a nominal emissivity of (1-0.11**6)= 0.99999. The degradation of the walls of the OBC to a reflectivity of 0.2 would still result in a 0.99999 emissivity. A degradation of the OBC signal due to emissivity degradation is therefore not likely. More likely is a degradation of the thermistors and associated electronics, which measure the temperature of the OBC, due to long term radiation effects. A change in the OBC emissivity or a change in the OBC thermometry will cause a change in the apparent gain of the detectors. This apparent change in the gain will be detected by the routine QA (monitoring the normalized gain). The level 1b software will compensate for the apparent decrease in gain by increasing the signal from the scene. This will show up as change in (observed-calc), where calc is the expected brightness temperature based on reliable external truth measurements. The routine monitoring and analysis of the bias in (obs-calc) is discussed in Appendix 3.

Are the LABB and OBC traceable to NIST?

Yes. The Large Area Blackbody output is NIST traceability based on contact thermometry using PRT's and its state of the art design. This is discussed in section 3 of the ATBD. In the AIRS temperature range between 200 and 350K and for the AIRS accuracy requirement reliance on contact thermometry and good design practice are adequate.

How is space view contamination by horizon proximity and moon addressed?

This is discussed in the section 3 as part of the space view selection algorithm. The validity of this algorithm has to be confirmed in orbit. The space view at 67 degree may well be permanently unusable. The strategy of multiple space view with selection optimization in orbit is also used on AMSU-B.

How does polarization effect the calibration? Is the difference between the calculated and the measured polarization understood?

The source and the effect of polarization in the AIRS calibration are discussed in Section 3. Every infrared radiometer which uses beam splitters, overcoated mirrors or gratings is to some extent polarizing. Any angular motion of these components relative to each other, e.g. the scan mirror rotation causes a modulation of the effective instrument transmission, which needs to be included in the calibration algorithm or be carried as an error term. . Polarization is very difficult to calculate for a

coarse grating used by AIRS. The agreement is surprisingly good most places. The directly measured polarization is used in all cases for the $p_r p_t$ correction term in the AIRS radiometric calibration equation.

How is detector striping (non uniform response to a uniform scene) corrected?

In the AIRS spectrometer all detectors (on linear arrays) share the same field-of-view, i.e. for radiometric calibration purposes AIRS acts like 2378 single channel spectrometers. The radiometric calibration process normalizes the gain of all detectors to a common (OBC) blackbody. Detector striping near the noise level is a common problem with linear and area array detectors.

When adjusting each detector gain (accounting for a different spectral interval) to the 308K blackbody, will the correction work for a cold scene (such as clouds) as well as for the warm scene?

This is discussed in Section 3. Correction terms have been developed based on the measured response from the LABB stabilized at 205K to 360K in steps of 15K to "adjust each detector" to give the correct output for cold and warm scenes. The accuracy of these correction terms has been directly demonstrated.

The presence of "popcorn noise" may degrade the radiometric calibration. How does the Level 1B software handle this?

The popcorn detection algorithm is described in Section 3.3. As of August 2006, popcorn type noise has been observed in only about 60 of the 2378 AIRS channels.

If a pop-event is detected, the entire scan line for this detector is flagged in the CalFlag array. Since the pop frequency is typically one pop in 500 seconds or less, the probability of two pops to occur one scan line or between space views (separated by 22 msec) is extremely small. The cause of "popping" is due to latice imperfections in the HgCd Te detector material which act as charge trapping sites. The charges accumulated in these sites is suddenly released, resulting in a current spike in the detector output. Lattice imperfections are changed by thermal cycling and strong radiation hits. Both occurred in November 2003, when a large solar flare necessitated the protective shutdown of AIRS. Popping events are detected by the Level 1b software by raised to popping flag for the effected scan line. Users of the AIRS data need to be aware that the intense radiation environment in the polar orbit, and radiation damage due to solar flares can cause large "pops" which are not caught by the de-glitcher in the AIRS on-board data system, and can turn "good channel" into a bad "popping" channel. Data users who cannot avoid using a channel which pops need to familiarize themselves with the radiometric validity flags generated routinely by the level 1b software, in particular the CalFlag.

Was the scan mirror non-uniformity calibrated in TVAC tests before launch?

Yes. This is discussed in the ATBD, section 3.4. The effect is sufficiently small to be negligible and still meet the AIRS absolute calibration requirements. Measurements during TVAC as function of scan angle have not detected unusual scan angle dependence of the calibration not explained by the $p_r p_t$ polarization effect.

Can changes in the scan mirror emissivity on-orbit for those positions on the mirror used to view the Earth be detected?

Yes. A change in the scan mirror emissivity for either Earth, OBC or space view positions will results in a change in the apparent detector gain. This is discussed in Appendix 2. A trend in the gain will show up as a trend in the time history plot. The trend in the gain will be highly correlated for channels in the same array. Emissivity non-uniformity also becomes apparent in the scan angle dependence of (obs-calc), again with a high correlation for channels in one module. As of August 2006, no such effects have been observed at the 100 mK level.

The effective centroids of the AIRS spectral channels are not exactly aligned. How does this effect the radiometric calibration?

The mean centroid of all AIRS channels is by definition the instrument boresight. The standard deviation of the centroids is 80 arcsec (2% of the diameter of the FOV, sometimes also referred to as 98% Cij). Each channel accurately measures the radiance appropriate to its FOV. However, if the scene is highly inhomogeneous, such as near clouds, then the small differences in the boresights result in differences, particularly for widely separated window channels, which can be considerably larger than the noise. Strictly speaking, this is not a calibration error, but an error in the interpretation of data in the presence of scene inhomogeneity. Scenes inhomogeneity is measured by the Level 1b software using channel pairs at 11 and 4 micron region and recorded for each footprint as Cij flags. Depending on the application the user has to decide if the spectrum can be used.
1) If the application uses the radiances from many channels, as does the Level 2 temperature and moisture retrieval algorithm, then mean boresight error is zero, i.e. there is no radiometric effect, but the relative misalignment of channels nominally viewing the same scene appears as additional random noise. The level 2 retrieval which is based on the simultaneous analysis of 320 channels optimally selected from the 2378 available channel, ignores the Cij flag.
2) If the application uses the mean of many observations from one channel, then there is no effect on the absolute accuracy of the calibration.

2. Questions about the spectral calibration.

AIRS proposes to monitor spectral calibration using Earth scene radiances rather than a well characterized, calibration source.

For the AIRS accuracy requirement the spectrally resolved features in the upwelling radiances are the one obvious and only reliable spectral calibration source. Table 4.2 shows the location of the selected spectral features.

How does contamination by clouds and thin cirrus affect "clear" scene spectral calibration?

No effect. Clouds, including cirrus clouds, will have little effect on the spectral calibration, since they lack the pronounced spectral signatures of the atmospheric gases over the narrow spectral range used in the frequency calibration.

How does the presence of clouds affect the scene spectral calibration?

AIRS is a pupil imaging spectrometer. In this design scene inhomogeneity does not affect the spectral calibration. The AIRS pupil imaging design is unique in a hyperspectral sIR sounder. Most spectrometers, including IASI (Infrared Atmospheric Sounder Interferometer) and the CrIS (Cross-track Interferometer Sounder) image the scene on the detector, with resulting scene inhomogeneity dependent spectral shifts.

Will the OBS be used in-orbit?

No. The OBS, described in Section 2.2 of the ATBD, allows estimation of focal plane position with an accuracy of about 1 micron, i.e. the equivalent of 1% of the SRF width. The OBC was very critical for pre-launch testing, where the use of other means of spectral calibration were impractical, and for system testing in TVAC at TRW, where there were no other spectral reference sources. In orbit the AIRS spectral calibration depends entirely on the location of features in the upwelling spectral radiance, as described in Section 4.

How often has the AMA be used in-orbit for spectral calibration?

The AMA, discussed in Section 2.1, allows motion in the dispersed, cross-dispersed and radial (focus) axis. The AMA was critical during the pre-launch calibration to optimize the position of the images of the entrance slits on the detector arrays (effectively the exit slit of the spectrometer) with a motion in the cross-dispersed direction. The AMA has not been used in orbits and there appears to be no need to do so.

Do changes in the grating temperature effect the spectral calibration? How does the grating constant vary with temperature? Can the required thermal stability be achieved?

This is discussed in Section 2.1. The effect of spectrometer temperature on the spectral calibration was measured in TVAC. A spectrometer temperature change causes an apparent shift in the focal plane position of 2.7 micron/degree K. Since the SRF width is equivalent to 100 microns, this corresponds to a shift of 2.7% of the SRF width or 22 ppm of the frequency per degree K temperature change. The effect is due to the expansion coefficient of the Aluminum of the grating, i.e. the grating constant changes. Since the temperature of the spectrometer is actively controlled relative to a set point at the 30 mK level, a 0.6 ppm modulation of the SRF centroids could be expected. This modulation is a factor of ten less than the SFR knowledge specification in the FRD.

The AIRS spectrometer has a time constant of 20 hours and the temperature is regulated at a set point to within 30mK. The spectral stability was tested under simulated orbital conditions. During the simulation of 24 hours "in orbit" the observed amplitude of the apparent focal plane motion was +/- 0.3 microns,

equivalent to 2.4 ppm.   Appendix 4. shows that a seasonal modulation of this magnitude can be inferred from (obs-calc), and can therefore be removed in off-line frequency calibration.

Can in-orbit changes in the SRF characteristic be detected? What can be done about them?

1. Yes. Is it likely to happen? No, as long as the spectrometer is maintained at its set point temperature the SRF shape is frozen into the design. There are no moving components in the grating array spectrometer that affect the SRF shape.
2. What will be done about it depends on the user:
   a) Operational assimilation: The operational direct assimilation software automatically applies the bias correction and proceeds with the assimilation. This removes the bias, but not any additional noise introduced by the change. There is little impact on the operational forecast system performance, as long as these change occur slowly (on a months timescale). Stability on this timescale is implicit in the AIRS thermal design.
   b) Climate Applications: The effect can be modeled based on the observed spectral dependence of changes in the bias and appropriate corrections can be applied to the SRF.

3. Questions about Level 1b Validation

What is the feedback between bias monitoring and level 1b software? Is the SST used for validation only or for vicarious calibration as well? What is the position of the AIRS instrument team on the usefulness of vicarious calibration for the on-orbit validation of instrument calibration?

The AIRS level 1b radiometric calibration uses the calibration coefficients derived from the pre-launch calibration. Vicarious calibration is not used. There is no feedback from SST observations to the calibration. Given the accurate radiometric characterization and stability of AIRS demonstrated during TVAC testing and now confirmed with three years of on-orbit trend analysis (Ref. 11 and 12), the use of vicarious calibration of any kind would totally compromise NIST traceability and climate research.

The process of vicarious validation differs from the process of vicarious calibration: Vicarious validation minimizes the residuals between measured radiances and radiances calculated based on ground-truth data by analyzing the root of the discrepancy and fixing the "error" at the root. This not only eliminates a bias under a specific condition, e.g. at 300K surface temperature or at a specific spectral frequency , but it decreases the bias at other conditions, e.g. much colder temperatures which cannot be readily validated via ground truth or a wide range of spectral frequencies. If spectral patterns in the residuals should at some point in the life of AIRS suggest a problem with the spectral calibration, appropriate corrections will be made in the software. This procedure eliminates bias and decreases the residual scatter. As of October 2006, vicarious validation has not been necessary for the radiometric calibration. Vicarious validation has been used to evaluate the SRFs, particularly changes due to channel spectra, but this is not a level 1b ATBD issue..